STUDIES OF MICROSTRIP ANTENNAE ON CYLINDRICAL STRUCTURES

A THESIS

SUBMITTED IN PARTIAL FULFILLMENT OF

THE REQUIREMENTS FOR THE DEGREE OF MASTER OF PHILOSOPHY

IN ELECTRONIC ENGINEERING IN THE GRADUATE SCHOOL OF

THE CHINESE UNIVERSITY OF HONG KONG

BY

TAN WAI PIN, B.SC.

DEPARTMENT OF ELECTRONIC ENGINEERING

THE CHINESE UNIVERSITY OF HONG KONG

December 1993

DEDICATION

TO MY PARENTS, C.L. TAN AND Y.L. LIM FOR THEIR LOVE.

ABSTRACT

This thesis presents the analysis of rectangular microstrip antennas wrapped either on the outside and inside surface of a metallic cylindrical duct. The present method is a full-wave analysis which rigorously solves the electromagnetic boundary value problem by retaining all field components. The electric surface current model is employed : The electric field and the surface electric current distribution are related by the spectral domain Green's function. Moment method is then used to determine entities like input impedance, mutual impedance, and resonant frequency.

Analysis of microstrip antennas on curved surfaces requires knowledge on special functions computation, for instance, Bessel functions and Hankel functions are needed for cylindrical bodies. Computation of complex argument Bessel function and Hankel function is a burden to the analysis of microstrip antennas on cylindrical surfaces, since existing routines available are either not accurate enough, restricted to real argument, or applicable for a relatively small range of argument. The first part of this thesis is devoted to the problem of computing integer order cylinder functions of wide range of complex argument, which makes subsequent analysis of microstrip antennas on cylindrical bodies possible .

The input impedance and mutual impedance of cylindrical-rectangular microstrip antennas are studied using this method. The Green's function in the spectral domain is derived by matching the boundary conditions on the interfaces. A homogeneous matrix equation is obtained from the integral equations by applying Galerkin's method, which is a special case of

moment method. The matrix equation is solved numerically for the surface current distribution, from which the input impedance and mutual impedance can be computed.

The complex resonant frequency and input impedance of rectangular microstrip antenna fabricated on the inner surface of a cylinder are also studied. A similar analysis method as that employed for studying cylindrical-rectangular microstrip antennas is used. The radiator is replaced by a surface current distribution on the interface between air and dielectric. The formulation will lead to a set of integral equations from which the current distribution on the patch can be evaluated. The set of integral equations is solved using Galerkin's method with sinusoidal basis functions. Muller's method is then used to locate the zero of the eigenvalue equation whose root is the complex resonant frequency. Both the real and the imaginary part of the complex resonant frequencies will be calculated with various dielectric substrate thicknesses. The input impedance is computed using a method similar to that of cylindrical-rectangular microstrip antenna.

Table of Contents

ACKNOWLEDGMENTS

I would like to express my cordial gratitude to my research supervisor Dr. K.Y. Lai for his guidance throughout the course of study.

Sincere thanks are due to Dr. K.M. Luk, who first introduced me the interesting topics of microstrip antennas.

Special thanks go to Mr. W.C. Chan, Mr. S.C. Lee, Dr. K.W. Leung, Mr. Terry, K.C. Lo, and Mr. K.W. Wong for their kindness, support and memorable days we shared during the years of study.

I also acknowledges my colleagues at the microwave laboratory, Mr. Y.P. Zhang and Dr. D. Li for helpful discussions.

Finally, I am indebted to Mr. T.S. Poon for his numerous helps during measurement process.

CHAPTER 1

INTRODUCTIONS

The concept of using microstrip antennas to provide printed radiating structures, which are electrically thin, lightweight, and low cost, is a relatively new development in antenna engineering. Although the concept of microstrip antenna was proposed by Deschamps [1] in 1953, no such practical antenna had been fabricated until early 70s' when a better theoretical model and low loss dielectric substrate was developed.

The key contributing factor for recent advances of microstrip antennas is the advent of electronic circuit miniaturization brought about by developments in large scale integration, fiber optics and sensor technology, which requires compact antennas that are compatible with integrated electronics. Microstrip antennas are now largely used due to their intrinsic advantages of low profile and weight, and conformity to curved surfaces.

In the early development phase, the analysis of microstrip antenna is based on various approximate methods like transmission line model and cavity model.

Transmission line model (TLM) [2] [3] [4] is the simplest approach of analyzing microstrip antennas, this method exploits the

analogy between a rectangular microstrip patch and a section of a transmission line. The equivalent transmission line of the rectangular patch is terminated with edge admittance at the two ends, input impedance is found by analyzing the transmission line network. Modifications to the TLM have been made to enable the analysis of mutual coupling, and analysis of non-rectangular patch shapes. The transmission line model is simple but it is still useful for first order engineering design.

A major breakthrough in microstrip antenna analysis has been the use of cavity model [5] in place of transmission line model. In this model, the microstrip antenna is considered as a cavity bounded by a magnetic walls along the edges and by electric walls on the metallic patch and ground plane. Several assumptions are made in cavity model, namely,

(1). The substrate must be very thin electrically that electric field has only z-component (ground plane on x-y plane), and magnetic field has only xy-components in the region bounded by the patch and the ground plane.

(2). The fields inside the cavity are independent of the z-coordinate for all frequencies of interest.

(3). The electric current on the patch must have no component normal to the edge at any point on the edges, implying a negligible tangential component of magnetic field along the edges.

With the assumptions made, the radiation patterns, input impedance, Q-factor, mutual impedance and resonant frequency of a microstrip antenna can be determined. This method is applicable to patch shapes for which the two-dimensional wave equation is separable. Cavity model gives satisfactory results when the substrate is thin compared to the operating wavelength.

Both transmission line model and cavity model do not consider the variation of field components along the normal direction between the patch and ground plane. This simplification will not cause significant errors to electrically thin microstrip antennas, however, this simplification is invalid for relatively thick microstrip antenna, say $h/\lambda \approx 0.1$. Hence, there is a need for an accurate full wave analysis method [6-9] for microstrip antenna. In full wave analysis methods, usually an integral equation is formulated and then moment method is used to solve the integral equation. Resonant frequency, input impedance, mutual impedance, and radiation patterns can be calculated using this method.

Microstrip antennas on curved surfaces are different from planar microstrip antennas in several aspects. In the analysis of planar microstrip antenna, it is usually assumed that the ground plane is flat

and is infinitely large, however, the ground plane for a microstrip antenna on curved surface is a finite surface with finite radius of curvature. The curvature of both the microstrip patch and the ground plane gives extra complexity to the analysis. Analysis of microstrip antennas on cylindrical bodies has been studied using cavity model [10] and moment method [11, 12].

In this thesis, full wave analysis is employed to solve some problems of rectangular microstrip antenna on cylindrical bodies.

Analysis of microstrip antennas on curved surfaces requires knowledge on special functions computation. For example, Bessel functions and Hankel functions are needed for cylindrical bodies; Mathieu functions are needed for elliptical cylinder; spherical Bessel functions are needed for spherical bodies. Computation of such special function is a burden to the analysis of microstrip antennas on curved surfaces especially when routines for calculating such special functions are unavailable. Chapter two of this thesis is devoted to the problem of computing integer order cylinder functions of a wide range of complex argument.

In chapter three, the input impedance of a cylindrical-rectangular microstrip antenna is considered using the spectral domain method. The spectral domain Green's function is obtained by subjecting the fields to the boundary conditions on the interfaces. A homogeneous matrix equation is derived by adding a test function and by applying Galerkin's

method which is a special type of moment method. The matrix equation is then solved numerically for the surface current components on the patch, from which input impedance can be calculated.

Chapter four gives an account of a method to calculate mutual impedance of rectangular microstrip antennas on cylindrical bodies. The method of analysis is basically an extension to that in chapter three.

In chapters five and six, the complex resonant frequency and input impedance of rectangular microstrip antenna wrapped inside a metallic cylinder are studied.

REFERENCE

1. G.A. Deschamps, "Microstrip microwave antennas," presented at the 3rd USAF Symposium on Antennas, 1953.

2. R.E. Munson, "conformal microstrip antennas and microstrip phased arrays," *IEEE Trans. Antennas Propagat.*, Vol. AP-22, pp. 77-78, Jan 1974.

3. A.G. Derneryd, "Linearly polarised microstrip antennas," *IEEE Trans. Antennas Propagat.*, Vol. AP-24, pp. 846-851, 1976.

4. A.G. Derneryd, "A theoretical investigation of the rectangular microstrip antenna element," *IEEE Trans. Antennas Propagat.*, Vol. AP-26, No.4, pp. 532-535, July 1978.

5. Y.T. Lo, D. Solomon, and W.F. Richards, "Theory and experiment on microstrip antennas," *IEEE Trans. Antennas Propagat.*, Vol. AP-27, pp. 137-145, 1979.

6. T. Itoh, "Analysis of microstrip resonators", *IEEE Trans. Microwave Theory Tech.*, Vol. MTT-22, pp. 946-952, 1974.

7. W.C. Chew, and J.A. Kong, "Resonance of non-axial symmetric modes in circular microstrip resonators," *J. Math. Phys.*, Vol. 21, pp. 2590-2598, 1980

8 W.C. Chew and Q. Liu, "Resonance frequency of rectangular microstrip patch," *IEEE Trans. Antennas Propagat.*, Vol. AP-36, pp. 1045-1057, 1988.

9. D.M. Pozar, "Input impedance and mutual coupling of rectangular microstrip antennas," *IEEE Trans. Antennas Propagat.*, Vol. AP-30, No. 6, pp. 1191-1196, Nov. 1982.

10. K.M. Luk, K.F. Lee and J.S. Dahele, "Analysis of the Cylindrical-rectangular patch antenna", *IEEE Trans. Antennas Propagat.*, vol. 37, No. 2, Feb 1989.

11. S.M. Ali, T.M. Habashy, J.F. Kiang and J.A. Kong, "Resonance in cylindrical-rectangular and wraparound microstrip structures", *IEEE Trans. Microwave Theory Tech.*, Vol. 37, No. 11, Nov 1989.

12. T.M. Habashy, S.M. Ali, and J.A. Kong, "Input impedance and radiation pattern if cylindrical-rectangular and wraparound microstrip antennas", *IEEE Trans. Antennas Propagat.* Vol. 38, No. 5, pp. 722-731, May 1990.

CHAPTER 2

COMPUTATION OF CYLINDER FUNCTIONS

1. INTRODUCTION

Bessel functions and Hankel functions of integer order occur as the solutions of many electromagnetic problems formulated in cylindrical coordinate system [4, Chap. 5]. Since the author is interested in the study of conformal antennas mounted on grounded substrate on metallic cylinder, where Bessel functions and Hankel functions which model standing waves and traveling waves are encountered frequently, and the range of the complex arguments of interest extends from zero to over several thousands in magnitude, which will normally have encountered problems of underflow or overflow in computation. Consequently, the accurate computation of Bessel functions and Hankel functions of a large range of complex argument is of importance. In this section, the term cylinder function is used to denote Bessel and Hankel functions collectively.

Amos [2] reports a sophisticated and portable code for Bessel functions. However, his underlying algorithm is not available for analysis. Du Toit [3] reports methods for computing Bessel functions of the first and second kind for integer orders and complex argument, but calculation of Hankel functions was not mentioned in his paper, also the argument range is limited by the computer's ability to handle large

number. Mason [6] has presented a convenient way of segmenting the complex z-plane where different algorithms can be applied. This chapter will give an account of works that extend previous works by adopting z-plane segmentation scheme similar to Mason's, and develop simple and efficient algorithms, and discussions on schemes for determining starting index for backward recurrence, ways to avoid exceeding permissible floating-point exponent range of the computer will also be covered.

The algorithm has been tested extensively and counter-checked with a number of existing routines. A FORTRAN-77 computer program implementing the algorithms presented is available from the author.

2. NEED OF COMPUTING CYLINDER FUNCTION OF COMPLEX ARGUMENTS

There are lots of well written routines for real argument cylinder functions, however there are relatively few routines available for computation of complex argument cylinder functions which are unavoidable in the study of microstrip antennas on cylindrical ground plane in spectral domain.

A typical Somerfeld integral to be evaluated numerically is of the following form :

$$Z_{np}^{zz} = -b\sum_{n=-\infty}^{\infty}\int_{-\infty}^{\infty}\tilde{J}_{zm}(-n,-k_z)\tilde{G}_{zz}\tilde{J}_{zp}(n,k_z)dk_z$$

where $\tilde{G}_{zz}$ is function of cylinder functions $C_n\left(\sqrt{k^2-k_z^2}b\right)$. The contour of integration cannot run on the x-axis from minus infinity to plus infinity, since the integrand possesses surface wave poles, a typical contour is shown in figure 2.1.

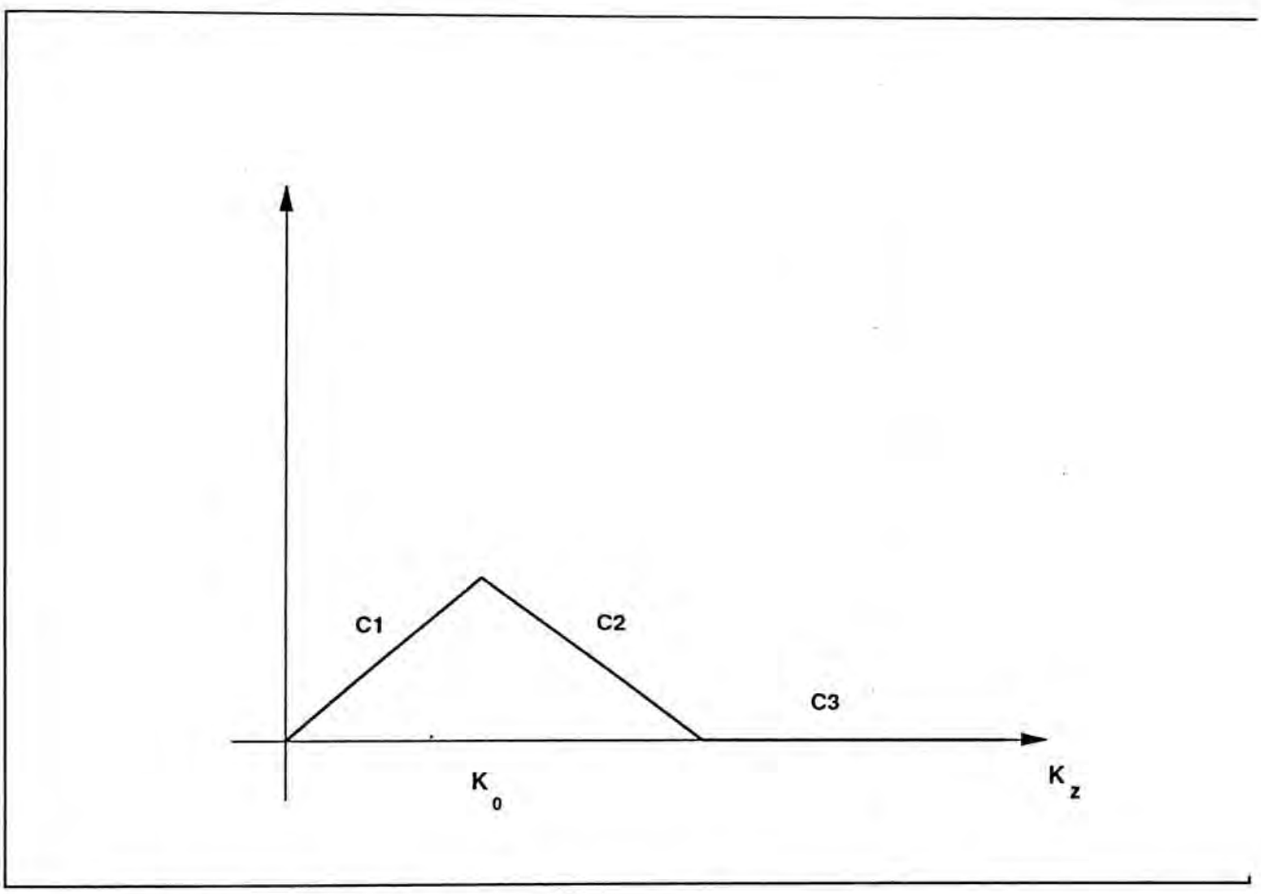

Figure 2.1 Contour of a typical Somerfled integral

The argument of $C_n\left(\sqrt{k^2-k_z^2}b\right)$ is complex on C1 and C2, purely imaginary in C3, so there is a need to compute cylinder functions with complex argument in general.

3. NEED OF COMPUTING HANKEL FUNCTIONS

As will be shown in chapter 3, the wave equation will be converted to a Bessel equation after taking Fourier transform, it is of the following form :

$$\frac{d^2y}{dx^2}+\frac{1}{x}\frac{dy}{dx}+\left(1-\frac{n^2}{x^2}\right)y=0 \qquad (2.1)$$

The general solution can be of either form :

$$y=C_1J_n(x)+C_2Y_n(x) \qquad (2.2)$$

$$y=C_3H_n^{(1)}(x)+C_4H_n^{(2)}(x) \qquad (2.3)$$

where C_1, C_2, C_3 and C_4 are constants, $J_n(x)$ is Bessel function, $Y_n(x)$ is Neumann function, $H_n^{(1)}(x)$ and $H_n^{(2)}(x)$ are Hankel functions of the first kind and second kind respectively. If either form is used, the Green's functions derived will be functions of $J_n(x)$ and $Y_n(x)$ only, or functions of $H_n^{(1)}(x)$ and $H_n^{(2)}(x)$ only, then it may appear that only the computation of $J_n(x)$ and $Y_n(x)$ or $H_n^{(1)}(x)$ and $H_n^{(2)}(x)$ are needed. If the solution takes the first form, it seems that the difficult problem of computing Hankel functions can be avoided.

It is absolutely correct in principle to write the Green's functions using $J_n(x)$ and $Y_n(x)$ or $H_n^{(1)}(x)$ and $H_n^{(2)}(x)$ only, but the other pair of cylinder functions are necessary in actual numerical computations of

the Green's functions, simply because the computer precision is not infinite. Here shows an example, the expression P_n/Q_n is very commonly encountered in the Green's functions :

$$\frac{P_n}{Q_n} = \frac{H_n^{(1)}(\kappa b)H_n^{(2)'}(\kappa a) - H_n^{(1)'}(\kappa a)H_n^{(2)}(\kappa b)}{H_n^{(1)'}(\kappa b)H_n^{(2)'}(\kappa a) - H_n^{(1)'}(\kappa a)H_n^{(2)'}(\kappa b)} \tag{2.4}$$

where κ may be complex. P_n/Q_n will incorrectly give zero divided by zero for large n, and $n >> |\kappa a|$, $n >> |\kappa b|$, which will certainly crash any machine. It is known the cylinder functions are related by the following expressions (similarly for the derivatives of the cylinder functions) :

$$\begin{aligned} H_n^{(1)}(z) &= J_n(z) + jY_n(z) \\ H_n^{(2)}(z) &= J_n(z) - jY_n(z) \end{aligned} \tag{2.5}$$

However, an alternate representation of P_n/Q_n derived using the above expression can avoid such type of numerical problems for $n >> |\kappa a|$, $n >> |\kappa b|$:

$$\frac{P_n}{Q_n} = \frac{J_n'(\kappa a)Y_n(\kappa b) - J_n(\kappa b)Y_n'(\kappa a)}{J_n'(\kappa a)Y_n'(\kappa b) - J_n'(\kappa b)Y_n'(\kappa a)} \tag{2.6}$$

On the other hand, the above representation (2.6) also suffers from similar numerical problems for $|\mathrm{Im}(\kappa a)| >> n, |\mathrm{Im}(\kappa b)| >> n$, in which it will incorrectly give zero divided by zero again. Under this circumstance, the first form will give the correct value of P_n/Q_n. It

turns out that both the representations of P_n/Q_n are necessary if the Green's functions are to be accurately computed.

The necessity of computing Bessel function, Neumann function, and two kinds of Hankel functions becomes clear now.

4. OUTLINE OF APPROACH

Hankel functions of the first and second kind are defined by :

$$\begin{aligned} H_n^{(1)}(z) &= J_n(z) + jY_n(z) \\ H_n^{(2)}(z) &= J_n(z) - jY_n(z) \end{aligned} \qquad (2.5)$$

where $j = \sqrt{-1}$

We are easily tempted to calculate $H_n^{(1)}(z)$ and $H_n^{(2)}(z)$ from $J_n(z)$ and $Y_n(z)$ using the above expressions. No problem will ever appear with small argument z, but if z has a sufficiently large positive or negative imaginary part, we have

$$\begin{aligned} J_n(z) &\to -jY_n(z) \quad , Im(z) >> 0 \\ J_n(z) &\to jY_n(z) \quad , Im(z) << 0 \end{aligned}$$

If the expressions (2.5) are used for computation of Hankel functions, the first one implies $H_n^{(1)}(z)$ equal to 0 and the second one implies $H_n^{(2)}(z)$ equal to 0, which are obviously wrong. This implies

that Hankel functions cannot be solely computed using expressions (2.5).

If z is small, a sequence of $J_n(z)$ are computed using Miller's algorithm, and the sequence of $Y_n(z)$ are calculated using forward recursion and those of $H_n^{(2)}(z)$ are calculated by using (2.5). If z is large, the sequence of $J_n(z)$ are calculated using backward recursion normalized by $J_0(z)$ which is calculated by evaluation of integral form, the sequence of $H_n^{(1)}(z)$ or $H_n^{(2)}(z)$ are calculated by first finding $H_0^{(1)}(z)$ and $H_1^{(1)}(z)$ using the integral form, and then using upward recursion afterwards, having $J_n(z)$ and $H_n^{(1)}(z)$ or $H_n^{(2)}(z)$, the sequence $Y_n(z)$ can be easily calculated by :

$$Y_n = jJ_n(z) - jH_n^{(1)}(z) \qquad (2.6a)$$

or

$$Y_n = -jJ_n(z) + jH_n^{(2)}(z) \qquad (2.6b)$$

In this manner, a combination of forward and backward recursion, which is difficult to implement, is not necessary to calculate the sequence of Neumann functions [6].

5. ALGORITHMS

The algorithms employed depend on segmentation of the z-plane. Figure 1 shows the division of regions.

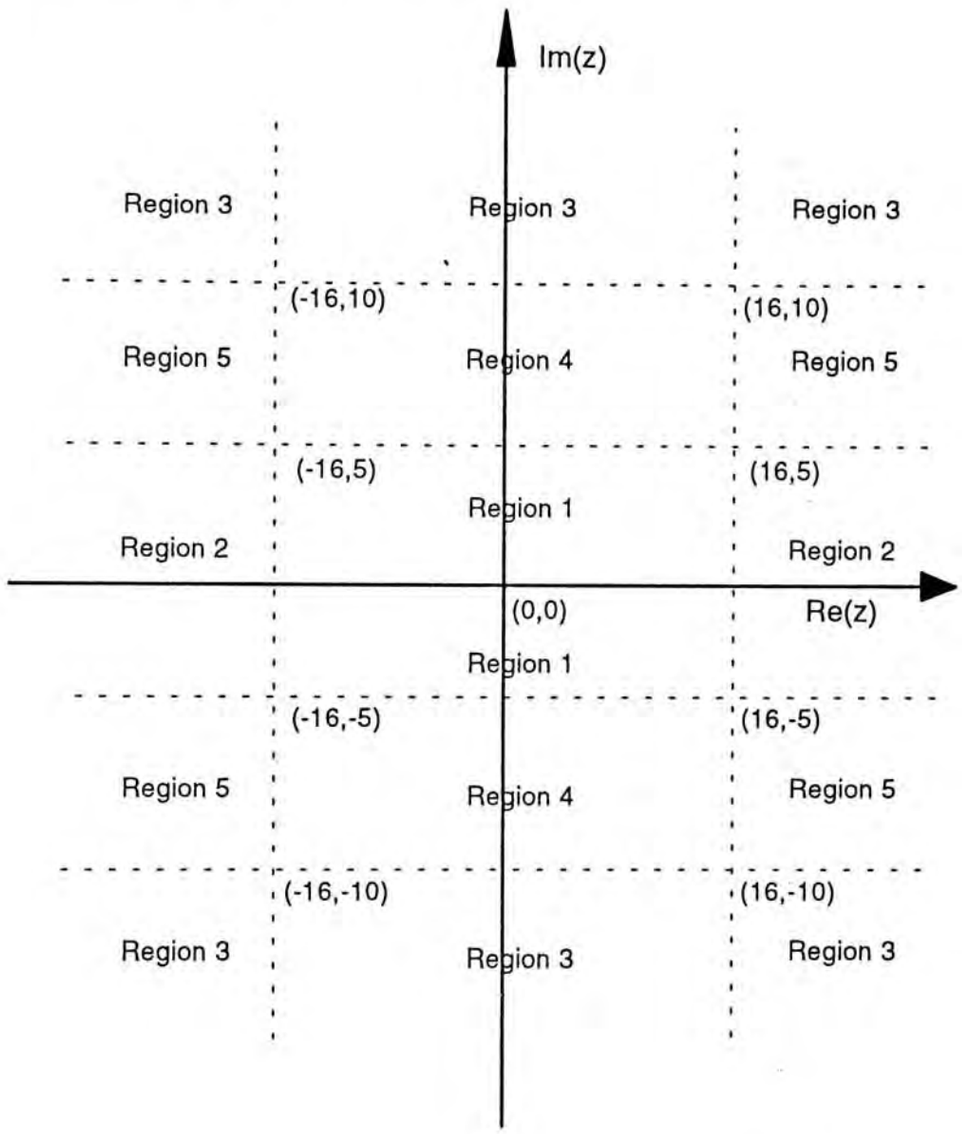

Figure 1 : Regional division of Complex z-plane

5.1. REGION 1 : |IM(Z)| < 5 AND |RE(Z)|<16 :

5.1.1. Computation of $J_n(z)$:

Miller's algorithm is used to find a sequence of Bessel functions $J_n(z)$, n=0,1,2...N. The sequence of Neumann functions $Y_n(z)$, n=0,1,2,...N, is calculated using the intermediate values during $J_n(z)$ computation.

The recurrence relation [1]

$$C_{n+1}(z) = \frac{2n}{z} C_n(z) - C_{n-1}(z) \qquad (2.7)$$

where $C_n(z)$ can be any cylinder function, enables the evaluation of all the orders for a given argument z, from any two known consecutive orders. However, the above statement was true for $J_n(z)$ if the computer had infinite precision arithmetic since $J_n(z)$ is a minimal solution to (2.7), any roundoff error will get amplified as the recurrence is going on in the increasing n direction. It is well known that for Bessel function $J_n(z)$, the recurrence is always stable in decreasing n. If two consecutive orders, say, $J_M(z)$ and $J_{M-1}(z)$ are assigned to zero and a small arbitrary number p, and the recurrence relation is executed in decreasing n direction, the error will diminish as the recurrence goes, a suitable normalization constant is needed to retrieve the whole sequence of $J_n(z)$ from a scaled sequence. The accuracy depends on the starting index M and the accuracy of the normalization constant.

The problems remaining are how to determine the normalization constant and the starting index M.

5.1.2. Determination of Starting Index M :

The starting index M for backward recursion is determined by the following expression which is adapted from an earlier version of Matlab (Note : The current version uses another scheme that occasionally gives an M < N for N >> z, which will obviously result in the wrong $J_n(z)$.

$$M = 17.1032 + 0.2639xN + 0.6487x|z| - 0.0018xNx|z| + 0.6457x\max(N,|z|) \quad (2.8)$$

It should be noted that Du Toit [3] reports a scheme that gives an optimal starting index, but it requires solution of a non-linear equation that is not as straightforward as the current approach.

5.1.3. Determination of Normalization Constant η :

The normalization constant η required can be obtained by using a truncated infinite series involving various orders of Bessel function.

The commonly used one is :

$$1 = J_0(z) + 2\sum_{k=1}^{\infty} J_{2k}(z) \quad (2.9)$$

If $\{\hat{J}_n(z)\}$ is the scaled sequence of Bessel functions obtained in backward recursion, then

$$\eta = \hat{J}_0(z) + 2\sum_{k=1}^{M/2}\hat{J}_{2k}(z) \qquad (2.9a)$$

However, if z is purely imaginary, the summation in equation (2.9) is not desirable since $J_{2k}(z)$ will oscillate between positive and negative values and it will be shown that such oscillation will cause numerical errors. The oscillation of values of $J_{2k}(z)$ between positive and negative values can be easily shown as follows.

Power series expansion for $J_n(z)$:

$$J_n(z) = (z/2)^n \sum_{k=0}^{\infty}\frac{(-z^2/4)^k}{k!\Gamma(n+k+1)} \qquad (2.10)$$

if $z = j\rho$,

$$J_{2n}(j\rho) = (\rho/2)^{2n}\sum_{k=0}^{\infty}\frac{(\rho^2/4)^k}{k!\Gamma(2n+k+1)}(-1)^n$$

$$J_{2n+2}(j\rho) = (\rho/2)^{2n+2}\sum_{k=0}^{\infty}\frac{(\rho^2/4)^k}{k!\Gamma(2n+k+3)}(-1)^{n+1}$$

It is seen that $J_{2n}(j\rho)$ and $J_{2n+2}(j\rho)$ are of different sign.

Besides, unless z is real, in which $J_n(z)$ is always less than 1 [1, eqn. 9.1.60], $J_n(z)$ can be much larger than 1. For imaginary z, the sequence of $J_{2k}(z)$ oscillates between positive and negative values

which can be very large, and equation (2.9) is to obtain the value 1 by adding and subtracting a large number of terms with large magnitudes, this process is particularly vulnerable to numerical errors since severe loss of precision may occur.

An infinite series that outperforms (2.9) for complex z is

$$\cos(z) = J_0(z) + 2\sum_{k=1}^{\infty}(-1)^k J_{2k}(z) \qquad (2.11)$$

then

$$\eta = \frac{\hat{J}_0(z) + 2\sum_{k=1}^{M/2}(-1)^k \hat{J}_{2k}(z)}{\cos(z)} \qquad (2.11a)$$

Obviously, equation (2.11) can avoid the problem caused by (2.9) if z is purely imaginary. Also, equation (2.11) converges faster than equation (2.9) for complex z, implying that normalization constant obtained by using (2.11a) is more accurate than that calculated using (2.9a) using the same number of terms, or equation (2.11) can give η with the same precision using less terms than equation (2.9). On the other hand, equation (2.9) performs better than equation (2.9) if z is real.

Table 1 gives some numerical examples about the convergence of equations (2.9) and (2.11). It is observed that for complex z, equation (2.11) gives faster convergence, as indicated by the smaller percentage error due to truncation than equation (2.9), equation (2.9)

gives faster or at least comparable convergence rate for real z. This implies that equation (2.11) performs better for complex z while equation (2.9) is more suitable for real z.

Argument z	Equation (2.9) Percentage Error	Equation (2.11) Percentage Error	N
5+5i	1.78e-13	4.79e-15	28
30+8i	8.99e-12	1.54e-14	60
30+80i	1.17e20	1.66e-14	136
80i	2.88e19	1.66e-14	128
2	2.22e-14	1.33e-14	20
5	0.00	1.96e-14	24
15	1.33e-13	3.65e-13	40
30	2.89e-10	1.62e-9	56
70	8.74e-12	1.05e-11	108

Table 1 : Percentage error due to truncated series of eqns (2.9) and (2.11)

So a criterion for choosing infinite series for normalization is that : if z is real, use equation (2.9a), otherwise use equation (2.11a).

5.1.4. Computation of $Y_n(z)$, $H_n^{(1)}(z)$ and $H_n^{(2)}(z)$

After evaluation of a sequence of $J_n(z)$, the sequence of $Y_n(z)$ can be efficiently calculated by the following method :

- First calculate $Y_0(z)$ using [ABRAMOWITZ et al 1964, eqn 9.1.89], noting that it can be calculated in the same backward recursion for $J_n(z)$.

$$Y_0(z)=\frac{2}{\pi}\left[\ln\left(\frac{z}{2}\right)+\gamma\right]J_0(z)-\frac{4}{\pi}\sum_{k=1}^{\infty}(-1)^k\frac{J_{2k}(z)}{k} \qquad (2.12)$$

- Calculate $Y_1(z)$ using either [1, eqn 9.1.88] or Wronskian relation [1, eqn 9.1.16].

$$Y_n(z)=-\frac{n!\left(\frac{z}{2}\right)^{-n}}{\pi}\sum_{k=0}^{n-1}\frac{\left(\frac{z}{2}\right)^k J_k(z)}{(n-k)k!}+\frac{2}{\pi}\left[\ln\left(\frac{z}{2}\right)-\psi(n+1)\right]J_n(z)$$

$$-\frac{2}{\pi}\sum_{k=1}^{\infty}(-1)^k\frac{(n+2k)J_{n+2k}(z)}{k(n+k)} \qquad (2.13)$$

$$\psi(1)=-\gamma,\quad \psi(n)=-\gamma+\sum_{k=1}^{n-1}k^{-1}\quad (n\geq 2)$$

Or

$$Y_1(z)=\left(J_1(z)Y_0(z)-\frac{2}{\pi z}\right)\frac{1}{J_0(z)} \qquad (2.14)$$

- Calculate $Y_n(z)$ using forward recursion from $Y_0(z)$ and $Y_1(z)$. $H_n^{(1)}(z)$ and $H_n^{(2)}(z)$ are calculated using equations (2.5).

$$H_n^{(1)}(z) = J_n(z) + jY_n(z)$$
$$H_n^{(2)}(z) = J_n(z) - jY_n(z) \qquad (2.5)$$

5.2. REGION 2 : $|Re(z)| \geq 16$ AND $|Im(z)| \leq 5$

In this region, the argument z can have a very large real part, making the starting index M for backward recursion computed by equation (2.8) very large, the computation time will be impractically long especially only Bessel functions of orders up to a relatively small number N, $N << |z|$, are needed.

If $N > |z|$, which is seldom encountered physically, similar algorithm as region 1 is employed to determine $J_n(z)$, n = 0,1,2,...,N.

However for real z or when $|Re(z)| >> |Im(z)|$, (note these conditions are automatically satisfied as z being in region 2), the general magnitude of $|J_n(z)|$ and $|Y_n(z)|$ is approximately constant for $n<|z|$, so the relative propagated error intrinsic to the recurrence relation is stable in increasing n direction [3] [7].

In order to apply forward recurrence for $J_n(z)$ and $Y_n(z)$, $J_0(z)$, $J_1(z)$, $Y_0(z)$ and $Y_1(z)$ are needed. They can be efficiently calculated by Hankel's asymptotic expansions [1, eqns. 9.2.5, 9.2.6].

$$J_n(z) \sim \sqrt{\frac{2}{\pi z}}\left\{P_n(z)\cos\left[z-\frac{n\pi}{2}-\frac{\pi}{4}\right]-Q_n(z)\sin\left[z-\frac{n\pi}{2}-\frac{\pi}{4}\right]\right\} \tag{2.15}$$

$$Y_n(z) \sim \sqrt{\frac{2}{\pi z}}\left\{P_n(z)\sin\left[z-\frac{n\pi}{2}-\frac{\pi}{4}\right]+Q_n(z)\cos\left[z-\frac{n\pi}{2}-\frac{\pi}{4}\right]\right\} \tag{2.16}$$

where

$$P_n(z) = 1+\sum_{k=1}^{\infty}\frac{(-1)^k(4n^2-1^2)(4n^2-3^2)\cdots(4n^2-(4k-1)^2)}{(2k)!2^{6k}z^{2k}}$$

$$Q_n(z) = \sum_{k=1}^{\infty}\frac{(-1)^{k+1}(4n^2-1^2)(4n^2-3^2)\cdots(4n^2-(4k-3)^2)}{(2k-1)!2^{6k-3}z^{2k-1}}$$

Hankel functions are calculated using same method as in region 1.

5.3. REGION 3 : $|\mathrm{Im}(z)| > 10$

5.3.1 Computation of $J_n(z)$:

$J_n(z)$ computation in this region also makes use of backward recursion, but have two numerical problems to solve, firstly, if the same infinite series (2.11) is used for normalization, and z is a very large complex number, the term cos(z) will overflow, failing equation (2.11a); secondly, if the argument z is very large, there will be numerical difficulties including the possible exceeding of exponent range of floating point number during $J_n(z)$ calculation.

To solve the first problem, normalization constant η is instead determined by the ratio of $\hat{J}_0(z)$ to $J_0(z)$, where $J_0(z)$ is calculated using integral form representation.

Before considering methods of fixing the second problem, two forms of integral representation of $J_n(z)$ will be considered. Commonly used integral form of $J_n(z)$ [6] is :

$$J_n(z) = \frac{1}{\pi}\int_0^{\pi} \cos(z\sin\theta - n\theta)\, d\theta \qquad (2.17)$$

In particular,

$$J_0(z) = \frac{1}{\pi}\int_0^{\pi} \cos(z\sin\theta)\, d\theta \qquad (2.17a)$$

$$J_1(z) = \frac{1}{\pi}\int_0^{\pi} \cos(z\sin\theta - \theta)\, d\theta \qquad (2.17b)$$

It will be shown shortly that an alternate form can be numerically evaluated slightly less efficiently but can be used to exponentially scaled the $J_n(z)$ sequence to tackle the problem of exceeding the exponent range of floating point number.

Consider the following integral form representation [5, p.149] :

$$J_n(z) = \frac{j^{-n}}{\pi}\int_0^{\pi} e^{jz\cos\theta} \cos(n\theta)\, d\theta \qquad (2.18)$$

In particular,

$$J_0(z) = \frac{1}{\pi}\int_0^{\pi} e^{jz\cos\theta}\, d\theta \qquad (2.18a)$$

$$J_1(z) = \frac{j^{-1}}{\pi}\int_0^{\pi} e^{jz\cos\theta}\cos(\theta)\, d\theta \qquad (2.18b)$$

The integrands of the two above integral form representations are plotted in graph (Figures 2 to 5). The following observations are made : The larger the value of $|\mathrm{Re}(z)|$ over $|\mathrm{Im}(z)|$, the greater the oscillations of the integrands; The integrand of (2.17a) is symmetrical about the line $t = \pi/2$, and the integrand of (2.18a) is the enlarged version of the portion of (2.17a) running from $t = 0$ to $t = \pi/2$. All these can be shown as follows :

Define $f(z,\theta) = \cos(z\sin\theta)$, then $f(z,\frac{\pi}{2}+\theta) = \cos(z\cos\theta)$

Define $g(z,\theta) = e^{jz\cos\theta}$, then if $|\mathrm{Im}(z)| >> 0$

$$g(z,\theta) = \cos(z\cos\theta) + j\sin(z\cos\theta)$$

$$\approx \begin{cases} \varepsilon(z,\theta) & 0 \le \theta \le \pi/2 \\ 2\cos(z\cos\theta) & \pi/2 \le \theta \le \pi \end{cases}$$

$$= \begin{cases} \varepsilon(z,\theta) & 0 \le \theta \le \pi/2 \\ 2f(z,\frac{\pi}{2}+\theta) & \pi/2 \le \theta \le \pi \end{cases}$$

where $\varepsilon(z,\theta) \approx 0$.

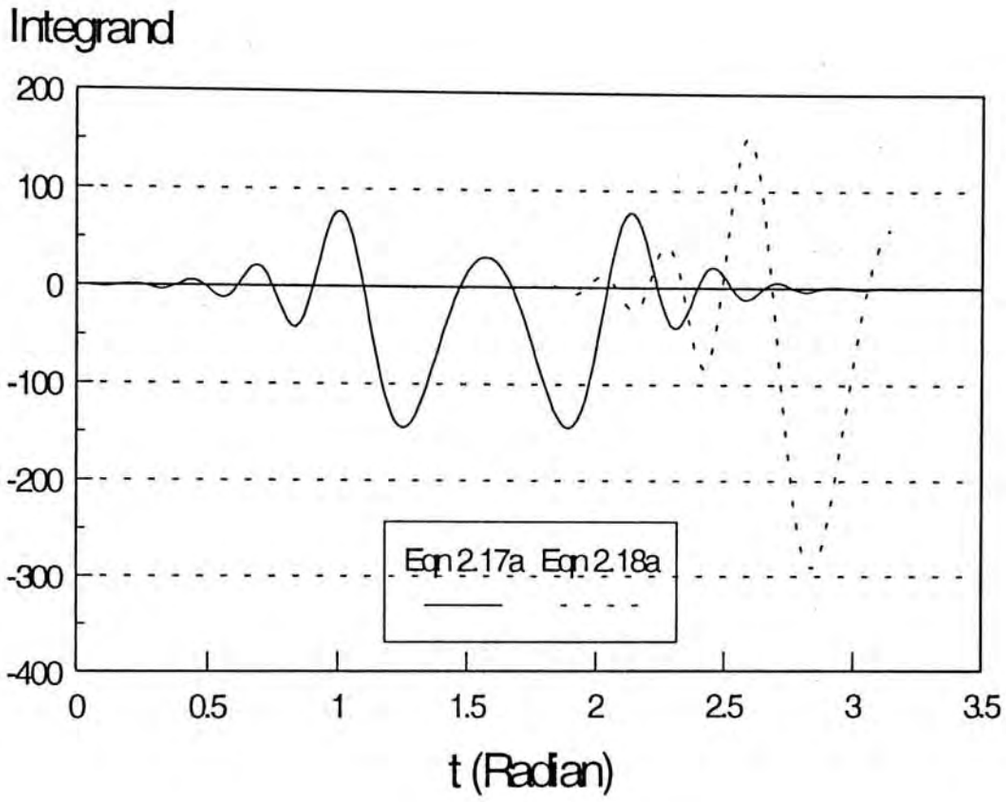

Figure 2 : Plot of Real Part of Integrands

$z = 30 + 6i$

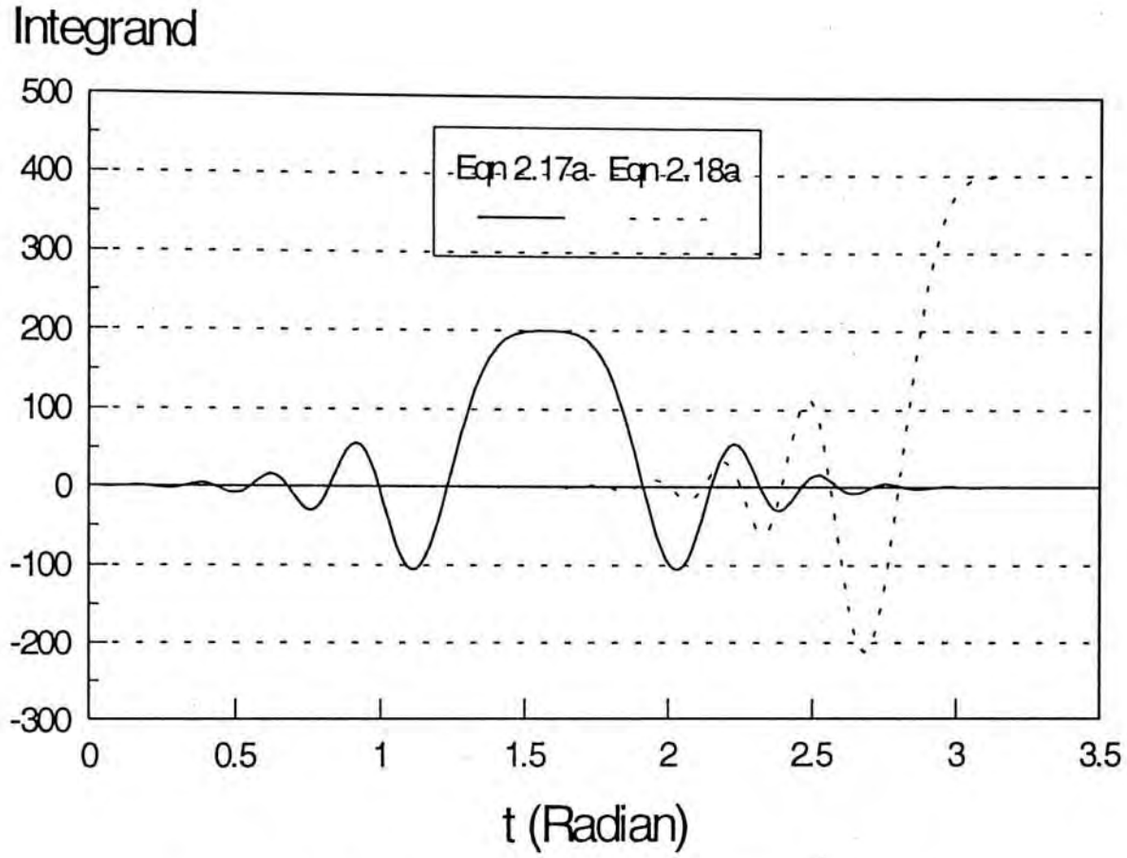

Figure 3 : Plot of Imaginary Part of Integrands

$z = 30 + 6\,i$

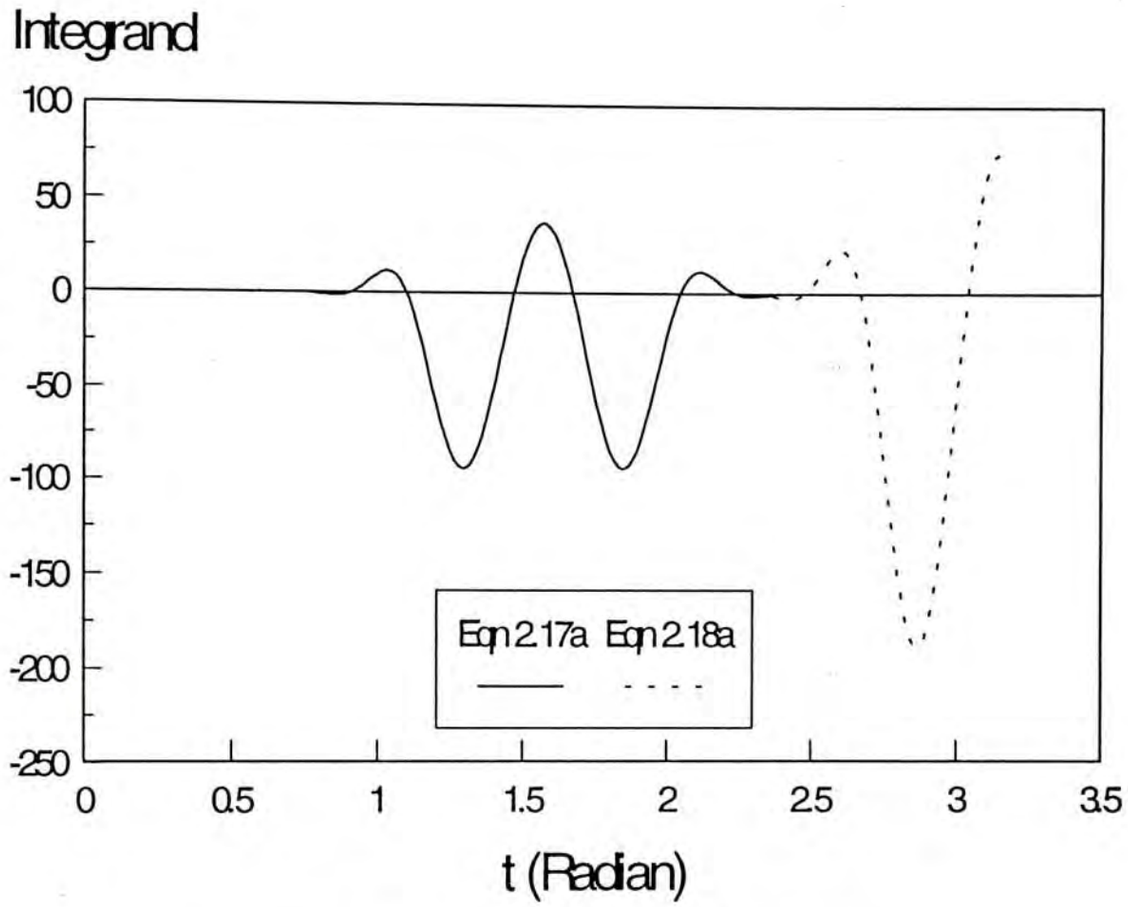

Figure 4 : Plot of Real Part of Integrands

$z = 30 + 20\,i$

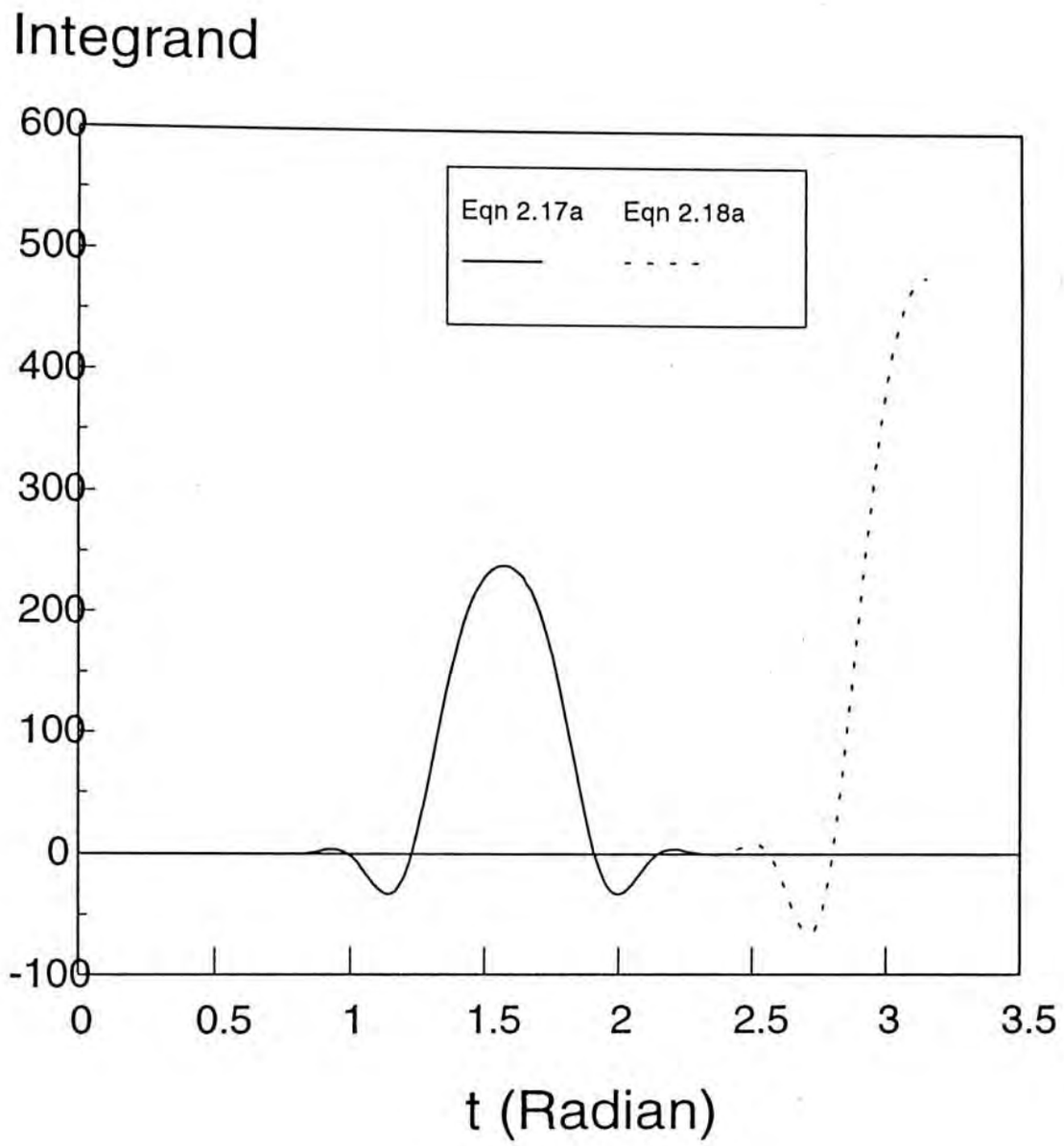

Figure 5 : Plot of Imaginary Part of Integrands

$z = 30 + 20\,i$

As a result, equation (2.17a) seems to give twice as many oscillations as that of equation (2.18a), actually for the range $0 \le \theta \le \pi/2$, there are oscillations symmetrical to that in the range $\pi/2 \le \theta \le \pi$ about the line $t = \pi/2$, but the amplitudes are so small that they can be virtually considered as zero. It is these small oscillations in the range $0 \le \theta \le \pi/2$, that makes (2.18a) slightly less accurate for numerical integration using Gauss-Legendre rule of same number of points. A typical value is 14 decimal places (Scientific notation) for (2.17a) and 13 places for (2.18a) using 96-point Gauss-Legendre rule.

Despite of the fact that form (2.18a) is slightly less accurate, it does provide a way of solving the problem of possible exceeding of exponent range which would otherwise require multiple precision routines or extended-range arithmetic routines similar to that of Smith [8] which are unavoidably slower in operation. Consider the integrand of (2.18), we have the following inequality :

$$\begin{aligned} \left|e^{jz\cos\theta}\cos(n\theta)\right| &= \left|e^{jz\cos\theta}\right|\left|\cos(n\theta)\right| \\ &\le \left|e^{jz\cos\theta}\right| \\ &= \left|e^{-\mathrm{Im}(z)\cos\theta}\right|\left|e^{j\mathrm{Re}(z)\cos\theta}\right| \\ &\le \left|e^{-\mathrm{Im}(z)\cos\theta}\right| \\ &\le \left|e^{-\mathrm{Im}(z)}\right| \end{aligned}$$

Hence $|J_n(z)| \leq |e^{-\mathrm{Im}(z)}|$. So if Im(z) >> 0, underflow may occur, while if Im(z) <<0, overflow may occur. However, if the term Im(z) in the exponent of the integrand is suppressed, no overflow or underflow may ever occur.

Since backward recursion with $J_0(z)$ for normalization is adopted, only equation (2.18a) has to be dealt with. Should there be any chances of overflow or underflow, instead of evaluating (2.18a), the following form is evaluated :

$$\tilde{J}_0(z) = \frac{1}{\pi}\int_0^{\pi} e^{jz\cos\theta - |\mathrm{Im}(z)|}\, d\theta \qquad (2.19)$$

$$\tilde{J}_0(z) = e^{-|\mathrm{Im}(z)|} J_0(z)$$

So this solves our problem, we can now compute a sequence of $J_n(z)$ by normalizing $\{\hat{J}_n(z)\}$ with $J_0(z)$ calculated using integral form, no matter how large the value $|z|$ may be, should $|z|$ be too large or too small, a sequence of exponentially scaled Bessel functions $\tilde{J}_n(z)$ is computed.

5.3.2 Computation of $H_n^{(1)}(z)$, $H_n^{(2)}(z)$ and $Y_n(z)$:

In this region, Hankel functions are calculated using forward recursion, and Neumann functions are calculated using relations (2.6a) or (2.6b).

If $|\mathrm{Im}(z)| \geq 0$, Hankel functions of the first kind $H_n^{(1)}(z)$ are computed, and Hankel function of the second kind $H_n^{(2)}(z)$ determined using

$$H_n^{(2)}(z) = 2J_n(z) - H_n^{(1)}(z)$$

If $|\mathrm{Im}(z)| < 0$, Hankel functions of the second kind $H_n^{(2)}(z)$ are computed, and Hankel function of the first kind $H_n^{(1)}(z)$ determined using

$$H_n^{(1)}(z) = 2J_n(z) - H_n^{(2)}(z)$$

To start the forward recursion, $H_0^{(i)}(z)$, where i = 1 or 2, is to be computed first. The integral form used is :

$$H_n^{(i)}(z) = \begin{cases} \dfrac{-2je^{-jn\pi}}{\sqrt{\pi}} \dfrac{(z/2)^n}{\Gamma(1/2+n)} \displaystyle\int_0^\infty \frac{t^{2n} e^{jz(t^2+1)^{1/2} - k|\mathrm{Im}(z)|}}{(t^2+1)^{1/2}} dt & ,i=1 \\ \dfrac{2j(-1)^n}{\sqrt{\pi}} \dfrac{(z/2)^n}{\Gamma(1/2+n)} \displaystyle\int_0^\infty \frac{t^{2n} e^{-jz(t^2+1)^{1/2} + k|\mathrm{Im}(z)|}}{(t^2+1)^{1/2}} dt & ,i=2 \end{cases} \tag{2.20}$$

where k=0, if no exponential scaling is necessary, k=1 otherwise. Whereas $H_1^{(i)}(z)$, i = 1 or 2, is determined by the Wronskian relations [5, p.144] :

$$H_1^{(1)}(z) = \frac{1}{J_0(z)} \left[\frac{2}{j\pi z} + J_1(z) H_0^{(1)} \right] \tag{2.21a}$$

$$H_1^{(2)}(z) = \frac{1}{J_0(z)}\left[J_1(z)H_0^{(2)} - \frac{2}{j\pi z}\right] \qquad (2.21b)$$

5.3.3 Determination of Point of Starting Exponential Scaling :

The starting value for argument z where exponential scaling begins is quite arbitrary, as long as beyond which underflow or overflow will occur. The algorithm described performs equally well if scaling is to be performed for all z. For double precision calculation, the criterion can be : $|\mathrm{Im}(z)| \geq 700$, however, since it is common to encounter expressions involving ratio of Bessel function, Neumann function and Hankel function, a safer criterion will be $|\mathrm{Im}(z)| \geq 300$, to make evaluation of such ratios possible.

5.4. REGION 4 : $|\mathrm{Re}(z)| < 16$ AND $5 < |\mathrm{Im}(z)| \leq 10$

If Hankel functions are not required, use similar algorithm as region 1 for computation of $J_n(z)$ and $Y_n(z)$. On the other hand, if Hankel functions are required, use algorithms as region 3, to avoid problems of failure of equations (2.5).

5.5. REGION 5 : $|\mathrm{Re}(z)| \geq 16$ AND $5 < |\mathrm{Im}(z)| \leq 10$

If Hankel functions are not required, use similar algorithm as region 2 for computation of $J_n(z)$ and $Y_n(z)$. On the other hand, if

Hankel functions are required, use algorithms as region 3, to avoid problems of failure of equations (2.5).

6. VERIFICATION

The program developed was tested using Mathematica 1.2. The results are tabulated in Table 2. It was that the algorithms described give good results, even for extremely large argument.

• Argument z	C_n	Present Method	Mathematica (*)
100+50j	$J_0(z)$	9.128743972068771 1E+19 +1.7312041196273807E+20j	9.128743972068766 5E+19 + 1.7312041196273764E+20j
	$Y_0(z)$	-1.7312041196273807E+20 +9.128743972068771 1E+19j	-1.7312041196273764E+20 + 9.128743972068766 5E+19j
	$H_0^{(1)}(z)$	3.1438393835330045E-25 -1.45434883185317710E-23j	0
	$H_0^{(2)}(z)$	1.8257487944137540E+20 +3.4624082392547613E+20j	1.8257487944137533E+20 + 3.4624082392547529E+20j
50+500j	$J_2(z)$	-2.3662844302103028E+215 -7.7090787695501840E+214j	-2.3662844302103892E+215 - 7.7090787695504895E+214j
	$Y_2(z)$	7.7090787695501840E+214 -2.3662844302103028E+215j	7.7090787695504895E+214 -2.3662844302103892E+215j
	$H_2^{(1)}(z)$	5.437305619626809E-220 +2.486579746282053E-219j	0
	$H_2^{(2)}(z)$	-4.7325688604206055E+215 -1.5418157539100367E+215j	-4.7325688604207784E+215 - 1.5418157539100979E+215j
30-800j	$J_5(z)$	-3.749853301190729E+345 -5.158546791246228E+344j	-3.7498533011908884E+345 - 5.158546791246495E+344j
	$Y_5(z)$	-5.158546791246228E+344 +3.749853301190729E+345j	-5.158546791246495E+344 + 3.7498533011908884E+345j
	$H_5^{(1)}(z)$	-7.499706602381458E+345 -1.031709358249245E+345j	-7.499706602381776 7E+345 - 1.031709358249299E+345j
	$H_5^{(2)}(z)$	-1.820476034215968E-350 -1.034520403238122E-349j	0
4+4j	$J_{40}(z)$	1.386856049661160E-30 - 2.740894488259289E-31j	1.3868560496611587E-30 - 2.74089448825929E-31j
	$Y_{40}(z)$	-5.510532505779805E+27 - 1.146467935944426E+27j	-5.510532505779683E+27 - 1.146467935945478E+27j
	$H_{40}^{(1)}(z)$	1.146467935944426E+27 - 5.510532505779805E+27j	1.146467935945478E27 - 5.510532505779683E+27j
	$H_{40}^{(2)}(z)$	-1.146467935944426E+27 + 5.510532505779805E+27j	-1.146467935945478E+27 + 5.510532505779683E+27j

50	$J_{10}(z)$	-0.1138478491494695	-0.1138478491494694
	$Y_{10}(z)$	5.7238971820533502E-03	0.005723897182053537
	$H_{10}^{(1)}(z)$	-0.1138478491494695 +5.7238971820533502E-03j	-0.1138478491494694 + 0.005723897182053537j
	$H_{10}^{(2)}(z)$	-0.1138478491494695 -5.7238971820533502E-03j	-0.1138478491494694 - 0.005723897182053537j

Table 2 : Tables of values of Cylinder functions

(*) : Since Mathematica can only calculate $J_n(z)$ and $Y_n(z)$, $H_n^{(1)}(z)$ and $H_n^{(2)}(z)$ are calculated using equations (2.5).

7. REFERENCE

1. M. Abramowitz, and I.A. Stegan, Eds., 1964, *Handbook of Mathematical Functions*, (New York : Dover Publications), Ch.9.

2. D.E. Amos, "A portable package for Bessel functions of a complex argument and nonnegative order", *ACM Transactions on Mathematical Software*, Vol. 12, no.3, 265-273. 1986.

3. C.F. Du Toit, "The numerical computation of Bessel functions of the first and second kind for integer orders and complex arguments", *IEEE Transactions on Antennas and Propagation*, Vol. 38, no.9, 1341-1349. 1990

4. R.F. Harrington, *Time-Harmonic Electromagnetic Fields*, (Prentice-Hall), Ch.5.

5. E. Jahnke, F. Emde, *Tables of Functions*, (New York : Dover) 1945.

6 J.P. Mason, "Cylindrical Bessel functions for a large range of complex arguments", *Computer Physics Communications*, **30**, 1-11. 1983

7 W.H. Press, B.P. Flannery, S.A. Teukolsky, And W.T. Vetterling, *Numerical Recipes,* (Cambridge University Press), 1989.

8 J.M. Smith, F.W.J. Olver, D.W. Lozier, "Extended-Range Arithmetic and Normalized Legendre Polynomials", *ACM Transactions on Mathematical Software*, Vol. 7, no.1, 93-105, March, 1981.

CHAPTER 3

INPUT IMPEDANCE OF CYLINDRICAL-RECTANGULAR MICROSTRIP ANTENNA

1. INTRODUCTION

One of the main advantages of microstrip patch antennas is that they can be made conformal to the surfaces on which they are mounted. For instance, rectangular microstrip patch antennas can be mounted on cylindrical surfaces like those on aircraft and spacecraft out of their conformity with the aerodynamical structure of such vehicles.

Such rectangular-cylindrical microstrip patch antennas have been the subject of several research efforts. Krowne [1] calculated the resonant frequencies using cavity model, Fonseca and Giarola [2] reported the radiation from the wraparound cylindrical microstrip antenna, and Ashkenazy et. al. [3] calculated the radiation patterns by using electric surface current model. Luk et. al. [4] reported a comprehensive analysis of a cylindrical-rectangular microstrip patch antenna which includes resonant frequencies, radiation patterns, input impedances and Q-factor using cavity model, however, the patch antenna must be electrically thin for cavity model to be valid. Habashy et. al. [9] reported the radiation and input impedance of cylindrical-rectangular and wraparound microstrip antenna using moment method.

In this chapter, an alternative method of calculating input impedance of probe-fed cylindrical-rectangular microstrip antenna is reported. The present method can be applied to microstrip antennas of thick substrates. Comparison of existing experimental results in literature shows excellent agreement.

2. FORMULATION

The geometry of the problem is shown in figures 1 and 2. A metallic cylinder of radius a is coated a layer of dielectric substrate whose thickness is t, relative permittivity ε_r, and relative permeability μ_0. A metallic patch, whose dimensions are $L \times W$ ($W = 2b\phi_0$), is printed on the surface of the dielectric substrate. The time convention $e^{j\omega t}$ is used throughout this chapter. In figure 1, region 1 is the region inside the dielectric substrate while region 2 is the free space within the cylinder.

Several assumptions are made :

1. Metallic Cylinder :
   - possession of perfect conductivity.
   - Cylinder's length is extended to infinite in both plus/minus z-direction.
2. Patch Radiator :
   - possession of perfect conductivity.
   - Zero thickness

3. Dielectric Layer :
   - Homogeneous.
   - Lossless.

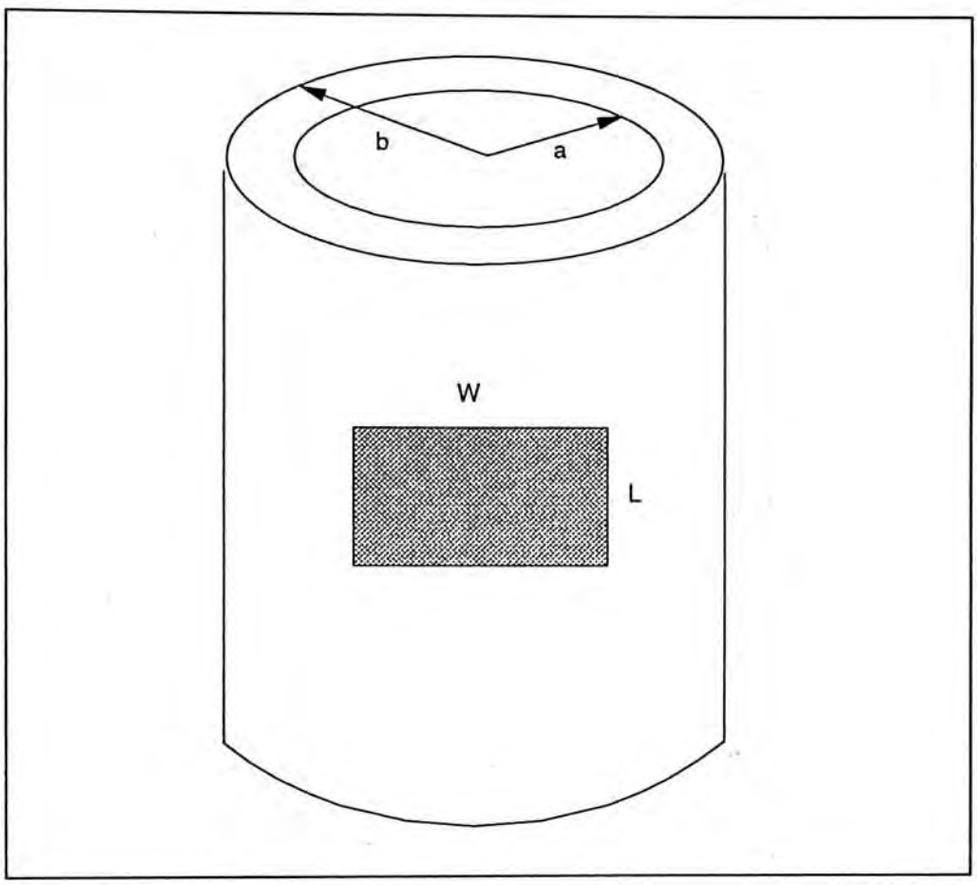

Figure 1 : Configuration of the Antenna

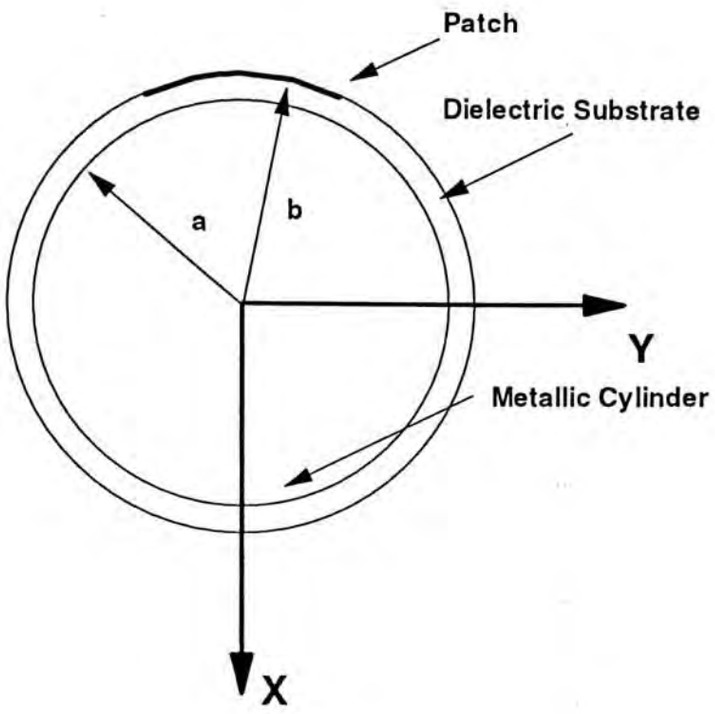

Figure 2 : Cross-sectional view of the antenna configuration

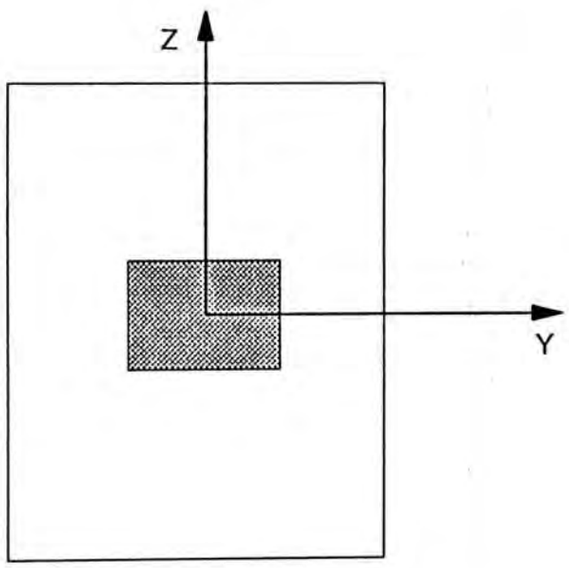

Figure 3 : Side view of the antenna configuration

For TM and TE decomposition of waves, we have :

$$\overline{A} = \Psi_m \hat{z}, \quad \overline{F} = 0 \quad (TM_z)$$
$$\overline{A} = 0, \quad \overline{F} = \Psi_e \hat{z} \quad (TE_z)$$

Hence we arrive at a set of scalar wave equations as follows :

$$\nabla^2 \begin{Bmatrix} \Psi_{mi} \\ \Psi_{ei} \end{Bmatrix} + k_i^2 \begin{Bmatrix} \Psi_{mi} \\ \Psi_{ei} \end{Bmatrix} = 0 \quad i = 1,2 \qquad (3.1)$$

where $k_1^2 = \varepsilon_r k_0^2$, and $k_2^2 = k_0^2$. The subscript i is used to denote region 1 or 2. A Fourier-Series-Fourier-Transform pair is defined similar to those of Harrington [7, p.246] and Ashkenazy et. al. [3] :

$$A(\rho,\phi,z) = \frac{1}{2\pi} \sum_{n=-\infty}^{\infty} \int_{-\infty}^{\infty} \tilde{A}(\rho,n,k_z) e^{j(n\phi - k_z z)} dk_z$$

$$\tilde{A}(\rho,n,k_z) = \frac{1}{2\pi} \int_0^{2\pi} \int_{-\infty}^{\infty} A(\rho,\phi,z) e^{-j(n\phi - k_z z)} dz d\phi \qquad (3.2)$$

Since an assumed current distribution on the patch is taken as the radiation source, so the source is introduced only through the boundary conditions. In other words, the scalar wave equations are homogeneous Helmholtz equations, which are expressed in cylindrical coordinate system and have the following form :

$$\frac{1}{\rho}\frac{\partial}{\partial\rho}\left(\rho\frac{\partial\psi_{mi}}{\partial\rho}\right) + \frac{1}{\rho^2}\frac{\partial^2\psi_{mi}}{\partial\phi^2} + \frac{\partial^2\psi_{mi}}{\partial z^2} + k^2\psi_{mi} = 0 \qquad (3.3)$$

and transformed using (3.2), the wave equations have the form of a Bessel differential equation :

$$\frac{d^2\tilde{\Psi}_{mi}}{d\rho^2}+\frac{1}{\rho}\frac{d\tilde{\Psi}_{mi}}{d\rho}+\left(k_{\rho i}^2-\frac{n^2}{\rho^2}\right)\tilde{\Psi}_{mi}=0 \qquad (3.4a)$$

$$\frac{d^2\tilde{\Psi}_{ei}}{d\rho^2}+\frac{1}{\rho}\frac{d\tilde{\Psi}_{ei}}{d\rho}+\left(k_{\rho i}^2-\frac{n^2}{\rho^2}\right)\tilde{\Psi}_{ei}=0 \qquad (3.4b)$$

where $k_{\rho i}^2 = k_i^2 - k_z^2$, i = 1, 2.

The solutions of the transformed wave equations in the 2 regions are :

Region 1:

$$\tilde{\Psi}_{m1}(\rho,n,k_z)=A_m(n,k_z)H_n^{(1)}(k_{\rho 1}\rho)+B_m(n,k_z)H_n^{(2)}(k_{\rho 1}\rho)$$
$$\tilde{\Psi}_{e1}(\rho,n,k_z)=A_e(n,k_z)H_n^{(1)}(k_{\rho 1}\rho)+B_e(n,k_z)H_n^{(2)}(k_{\rho 1}\rho) \qquad (3.5)$$

Region 2:

$$\tilde{\Psi}_{m2}(\rho,n,k_z)=C_m(n,k_z)H_n^{(2)}(k_{\rho 2}\rho)$$
$$\tilde{\Psi}_{e2}(\rho,n,k_z)=C_e(n,k_z)H_n^{(2)}(k_{\rho 2}\rho) \qquad (3.6)$$

The solution in (3.5) and (3.6) are just one among several possible solutions of the Bessel functions, alternatively the fields in region 1 can be expressed in terms of combination of Bessel function and Neumann function, the ultimate result is independent of the solution selected here.

We can always express the field components in terms of the vector electric potential and vector magnetic potential [10], and we can employ the boundary conditions to eliminate the coefficients. The boundary conditions are :

1. Tangential electric field vanishes on the surface of a cylinder.
2. Tangential electric field is continuous across the interface of air and dielectric substrate.
3. The discontinuity of the tangential magnetic field across the interface of air and dielectric substrate is equal to the surface current.

Or in mathematical form :

1. $\hat{\rho} \times \overline{E}_1 = 0$ on the surface $\rho = a$
2. $\hat{\rho} \times (\overline{E}_2 - \overline{E}_1) = 0$ on the surface $\rho = a$
3. $\hat{\rho} \times (\overline{H}_2 - \overline{H}_1) = \overline{J}_s$ on the surface $\rho = b$

(3.7)

By matching the boundary conditions on the tangential components of electric fields (E_z, E_ϕ) at the surface of the cylinder which is assumed to be perfectly conducting, we obtain the following relationships between the spectral amplitudes A_m and B_m, A_e and B_e :

$$\alpha_m = -\frac{B_m}{A_m} = \frac{H_n^{(1)}(k_{\rho 1} a)}{H_n^{(2)}(k_{\rho 1} a)}$$

$$\alpha_e = -\frac{B_e}{A_e} = \frac{H_n^{(1)'}(k_{\rho 1}a)}{H_n^{(2)'}(k_{\rho 1}a)} \qquad (3.6)$$

The relations between the inward radial propagating and outward radial propagating waves inside the dielectric substrate are thus determined.

Similarly by matching the boundary conditions on the tangential components of electric fields at the patch's surface, we obtain the followings :

$$A_m = \beta_m C_m$$
$$A_e = \gamma_m C_m + \gamma_e C_e \qquad (3.7)$$

where

$$\beta_m = \left(\frac{k_{\rho 2}}{k_{\rho 1}}\right)^2 \varepsilon_r \frac{H_n^{(2)}(k_{\rho 2}b)}{T_m(b)}$$

$$\gamma_m = \frac{k_0^2(\varepsilon_r - 1)}{j\omega\varepsilon_0 b} \cdot \frac{nk_z}{k_{\rho 1}^2} \cdot \frac{H_n^{(2)}(k_{\rho 2}b)}{T_e'(b)}$$

$$\gamma_e = k_{\rho 2} \frac{H_n^{(2)'}(k_{\rho 2}b)}{T_e'(b)}$$

$$T_m(b) = H_n^{(1)}(k_{\rho 1}b) - \alpha_m H_n^{(2)}(k_{\rho 1}b)$$

$$T_e'(b) = k_{\rho 1}\left[H_n^{(1)'}(k_{\rho 1}b) - \alpha_e H_n^{(2)'}(k_{\rho 1}b)\right]$$

Hence, we arrive at the relationship between waves inside the dielectric region and those in free space.

An expression relating the current on the patch to the spectral amplitudes of the fields in free space is to be derived next. It can be achieved by matching the discontinuity in the tangential components of the magnetic field to the surface current distribution.

The following expression is found :

$$\begin{bmatrix} \tilde{J}_{sz}(b,n,k_z) \\ \tilde{J}_{s\phi}(b,n,k_z) \end{bmatrix} = \overline{\overline{M}} \begin{bmatrix} C_m \\ C_e \end{bmatrix} \qquad (3.8)$$

where $\tilde{J}_{s\phi}$ is the transformed ϕ-directed surface current, and $\tilde{J}_{sz}$ is the transformed z-directed surface current, and

$$\overline{\overline{M}} = \begin{bmatrix} M_{11} & M_{12} \\ M_{21} & M_{22} \end{bmatrix}$$

$$M_{11} = -k_{\rho 2} H_n^{(2)'}(k_{\rho 2} b) + \beta_m T_m'(b) - \frac{n k_z \gamma_m T_e(b)}{j\omega\mu_0 b}$$

$$M_{12} = \frac{-n k_z}{j\omega\mu_0 b}\left[-H_n^{(2)}(k_{\rho 2} b) + \gamma_e T_e(b)\right]$$

$$M_{21} = \frac{k_{\rho 1}^2}{j\omega\mu_0}\gamma_m T_e(b)$$

$$M_{22} = \frac{1}{j\omega\mu_0}\left[-k_{\rho 2}^2 H_n^{(2)}(k_{\rho 2} b) + k_{\rho 1}^2 \gamma_e T_e(b)\right]$$

Hence we have all the information to relate the surface current distributions to the field components on both the dielectric region and the free space. If input impedance is desired, we shall refer to the fields inside the dielectric. The transformed electric field components in region 1 (dielectric) are shown to be related to the field spectral amplitudes as follows :

$$\begin{bmatrix} \tilde{E}_{z1}(\rho, n, k_z) \\ \tilde{E}_{\phi 1}(\rho, n, k_z) \\ \tilde{E}_{\rho 1}(\rho, n, k_z) \end{bmatrix} = \begin{bmatrix} T_{11} & T_{12} \\ T_{21} & T_{22} \\ T_{31} & T_{32} \end{bmatrix} \begin{bmatrix} C_m \\ C_e \end{bmatrix} \qquad (3.9)$$

where

$$T_{11} = \frac{k_{\rho 1}^2}{j\omega\varepsilon_r\varepsilon_0} T_m(\rho)\beta_m$$

$$T_{12} = 0$$

$$T_{21} = \frac{nk_z}{j\omega\varepsilon_0\varepsilon_r\rho} T_m(\rho)\beta_m + \gamma_m T_e'(\rho)$$

$$T_{22} = \gamma_e T_e'(\rho)$$

$$T_{31} = \frac{-k_z}{\omega\varepsilon_0\varepsilon_r} T_m'(\rho)\beta_m - \frac{jn\gamma_m}{\rho} T_e'(\rho)$$

$$T_{32} = -\frac{jn\gamma_e}{\rho} T_e'(\rho)$$

From (3.8) and (3.9), we can obtain the relationship between the patch current distribution and the electric field on the patch in the spectral domain, and hence we can derive the spectral domain Green's function :

$$\begin{bmatrix} \tilde{E}_z(\rho,n,k_z) \\ \tilde{E}_\phi(\rho,n,k_z) \\ \tilde{E}_\rho(\rho,n,k_z) \end{bmatrix} = \begin{bmatrix} \tilde{G}_{zz} & \tilde{G}_{z\phi} \\ \tilde{G}_{\phi z} & \tilde{G}_{\phi\phi} \\ \tilde{G}_{\rho z} & \tilde{G}_{\rho\phi} \end{bmatrix} \begin{bmatrix} \tilde{J}_{sz} \\ \tilde{J}_{s\phi} \end{bmatrix} \qquad (3.10)$$

where

$$\begin{bmatrix} \tilde{G}_{zz} & \tilde{G}_{z\phi} \\ \tilde{G}_{\phi z} & \tilde{G}_{\phi\phi} \\ \tilde{G}_{\rho z} & \tilde{G}_{\rho\phi} \end{bmatrix} = \begin{bmatrix} T_{11} & T_{12} \\ T_{21} & T_{22} \\ T_{31} & T_{32} \end{bmatrix} \begin{bmatrix} M_{11} & M_{12} \\ M_{21} & M_{22} \end{bmatrix}^{-1}$$

$$= \frac{1}{\Delta} \begin{bmatrix} T_{11}M_{22} - T_{12}M_{21} & -T_{11}M_{12} + T_{12}M_{11} \\ T_{21}M_{22} - T_{22}M_{21} & -T_{21}M_{12} + T_{22}M_{11} \\ T_{31}M_{22} - T_{32}M_{21} & -T_{31}M_{12} + T_{32}M_{11} \end{bmatrix}$$

and Δ is the determinant of $\overline{\overline{M}}$.

The space domain electric field in region 1 can be expressed in terms of the spectral domain Green's functions and the surface current components as follows :

$$\overline{E}_1(\rho,\phi,z)=\frac{1}{2\pi}\sum_{n=-\infty}^{\infty}\int_{-\infty}^{\infty}\left(\tilde{G}_{zz}\hat{z}+\tilde{G}_{\phi z}\hat{\phi}+\tilde{G}_{\rho z}\hat{z}\right)\tilde{J}_{sz}e^{j(n\phi-k_z z)}dk_z$$

$$+\frac{1}{2\pi}\sum_{n=-\infty}^{\infty}\int_{-\infty}^{\infty}\left(\tilde{G}_{z\phi}\hat{z}+\tilde{G}_{\phi\phi}\hat{\phi}+\tilde{G}_{\rho\phi}\hat{z}\right)\tilde{J}_{s\phi}e^{j(n\phi-k_z z)}dk_z \qquad (3.11)$$

The above equation relates the unknown electric field inside the dielectric to the unknown surface current distributions. In order to solve for the unknowns, Galerkin's method is employed (See appendix A for more information). The surface current on the patch is first expanded in terms of known basis functions with unknown coefficients, and after transforming it using (2), we have :

$$\tilde{J}_{sz}(n,k_z)=\sum_{p=1}^{N_z}I_{zp}\tilde{J}_{zp}(n,k_z)$$

$$\tilde{J}_{s\phi}(n,k_z)=\sum_{q=1}^{N_\phi}I_{\phi q}\tilde{J}_{\phi q}(n,k_z) \qquad (3.12)$$

Substituting (12) into (11), we have the following expression :

$$\overline{E}_1(\rho,\phi,z)=\sum_{p=1}^{N_z}I_{zp}\overline{E}_{zp}+\sum_{q=1}^{N_\phi}I_{\phi q}\overline{E}_{\phi q} \qquad (3.13)$$

where

$$\overline{E}_{zp}=\frac{1}{2\pi}\sum_{n=-\infty}^{\infty}\int_{-\infty}^{\infty}\left(\tilde{G}_{zz}\hat{z}+\tilde{G}_{\phi z}\hat{\phi}+\tilde{G}_{\rho z}\hat{\rho}\right)\tilde{J}_{zp}e^{j(n\phi-k_z z)}dk_z$$

$$\overline{E}_{\phi p}=\frac{1}{2\pi}\sum_{n=-\infty}^{\infty}\int_{-\infty}^{\infty}\left(\tilde{G}_{z\phi}\hat{z}+\tilde{G}_{\phi\phi}\hat{\phi}+\tilde{G}_{\rho\phi}\hat{\rho}\right)\tilde{J}_{\phi q}e^{j(n\phi-k_z z)}dk_z$$

Since the tangential electric fields on the patch is zero, we have :

$$\overline{E}_t(\overline{J}_s) + \overline{E}_i = 0 \tag{3.14}$$

The inner product of $\overline{a}$ and $\overline{b}$ is defined as follows :

$$\langle \overline{a}, \overline{b} \rangle = \iint_S \overline{a} \cdot \overline{b}\, dS \tag{3.15}$$

By taking inner product with the same set of basis functions (i.e. $J_{zm}, J_{\phi m}$), we have

$$\iint_S \sum_{p=1}^{N_z} I_{zp} \overline{E}_{zp} \cdot \overline{J}_{zm} ds + \iint_S \sum_{q=1}^{N_\phi} I_{\phi q} \overline{E}_{\phi q} \cdot \overline{J}_{zm} ds + \iint_S \overline{E}_i \cdot \overline{J}_{zm} ds = 0$$

$$\iint_S \sum_{p=1}^{N_z} I_{zp} \overline{E}_{zp} \cdot \overline{J}_{\phi m} ds + \iint_S \sum_{q=1}^{N_\phi} I_{\phi q} \overline{E}_{\phi q} \cdot \overline{J}_{\phi m} ds + \iint_S \overline{E}_i \cdot \overline{J}_{\phi m} ds = 0 \tag{3.16}$$

The above equations can be rewritten as a set of linear equations :

$$\sum_{p=1}^{N_z} I_{zp} Z_{mp}^{zz} + \sum_{q=1}^{N_\phi} I_{\phi q} Z_{mq}^{z\phi} = V_{zm}, \quad m = 1,2,\cdots,N_z$$

$$\sum_{p=1}^{N_z} I_{zp} Z_{np}^{\phi z} + \sum_{q=1}^{N_\phi} I_{\phi q} Z_{mq}^{\phi\phi} = V_{\phi m}, \quad m = 1,2,\cdots,N_\phi \qquad (3.17)$$

where

$$Z_{mp}^{zz} = -\iint_S \bar{E}_{zp} \cdot \bar{J}_{zm} b d\phi dz$$

$$= -b \sum_{n=-\infty}^{\infty} \int_{-\infty}^{\infty} \tilde{J}_{zm}(-n,-k_z) \tilde{G}_{zz} \tilde{J}_{zp}(n,k_z) dk_z$$

Similarly,

$$Z_{mq}^{z\phi} = -b \sum_{n=-\infty}^{\infty} \int_{-\infty}^{\infty} \tilde{J}_{zm}(-n,-k_z) \tilde{G}_{z\phi} \tilde{J}_{\phi q}(n,k_z) dk_z$$

$$Z_{mp}^{\phi z} = -b \sum_{n=-\infty}^{\infty} \int_{-\infty}^{\infty} \tilde{J}_{\phi m}(-n,-k_z) \tilde{G}_{\phi z} \tilde{J}_{zp}(n,k_z) dk_z$$

$$Z_{mq}^{\phi\phi} = -b \sum_{n=-\infty}^{\infty} \int_{-\infty}^{\infty} \tilde{J}_{\phi m}(-n,-k_z) \tilde{G}_{\phi\phi} \tilde{J}_{\phi q}(n,k_z) dk_z$$

By using reciprocity theorem, and assuming the feed current is modeled by a delta function,

$$V_{zm} = \int_S \bar{E}_i \cdot \bar{J}_{zm} ds = \int_v \bar{J}_i \cdot \bar{E}_{zm} dv$$

$$= \int_a^b \int_0^{2\pi} \int_{-\infty}^{\infty} \frac{1}{\rho} \delta(\phi - \phi_s) \delta(z - z_s) \frac{1}{2\pi} \sum_{n=-\infty}^{\infty} \int_{-\infty}^{\infty} \tilde{G}_{\rho z} \tilde{J}_{zm}(n, k_z) e^{j(n\phi_s - k_z z_s)} dk_z \rho d\rho d\theta dz$$

$$= \sum_{n=-\infty}^{\infty} \int_a^b \int_{-\infty}^{\infty} \tilde{G}_{\rho z} \tilde{J}_{zm}(n, k_z) e^{j(n\phi_s - k_z z_s)} dk_z d\rho$$

Similarly,

$$V_{\phi m} = \int_S \bar{E}_i \cdot \bar{J}_{\phi m} ds$$

$$= \sum_{n=-\infty}^{\infty} \int_a^b \int_{-\infty}^{\infty} \tilde{G}_{\rho\phi} \tilde{J}_{\phi m}(n, k_z) e^{j(n\phi_s - k_z z_s)} dk_z d\rho$$

We choose the sinusoidal function as the entire domain basis functions.

$$\bar{J}_s = \hat{z} \sum_{p=1}^{N_z} I_{zp} J_{zp} + \hat{\phi} \sum_{q=1}^{N_\phi} I_{\phi q} J_{\phi q} \qquad (3.18)$$

where

$$J_{zp} = \sin\left[\frac{2p-1}{L}\left(z - \frac{L}{2}\right)\pi\right]$$

$$J_{\phi q} = \sin\left[\frac{2q-1}{2\phi_0}(\phi - \phi_0)\pi\right]$$

Equation (3.17) can be concisely written as :

$$[Z][I]=[V] \tag{3.19}$$

and then the current vector can be found by either calculating the inverse of the Z-matrix or using LU-decomposition.

$$[I]=[Z]^{-1}[V] \tag{3.20}$$

where

$$[I]=\begin{bmatrix}[I_{zp}]\\ [I_{\phi q}]\end{bmatrix}$$

The input impedance is calculated using the following equation [10].

$$Z_{in}=\frac{-1}{I_i^2}\iiint_v \bar{E}\cdot\bar{J}_i dv$$

$$=-\sum_{n=1}^{N} I_n V_n \tag{3.21}$$

where I_n is the element of current vector [I], and V_n is the corresponding element of voltage vector [V].

3. DISCUSSION

The input impedance calculated is checked with experimental data from Dahele et. al. Figure 4 shows the calculated and measured values of the input impedances of the TE_{01} mode as a function of frequency. The configuration is : A microstrip patch of dimensions 3 cm length by 4 cm width, fed by a coaxial feed at z'=-0.01, built on a metallic cylinder of 5 cm radius, the dielectric substrate of $\varepsilon_r = 2.32$ and thickness of 0.0795 cm

is used. Excellent agreement between theory and experiment is achieved. The measured resonant frequency is 3.170 GHz, while the theoretical value is 3.201 GHz. The theoretical resonant frequencies differ from those measured by Dahele only about 0.98%, which is better than the value of 1.9% obtained by Dahele et. al. that makes use of the cavity model.

Figure 5 shows the input impedance against frequency for a thicker substrate (h=0.159 cm). Again excellent agreements between theory and experiment is obtained. The differences between the theoretical resonant frequency and the measurement is only 0.16%, compared to the 1.1% obtained by Dahele et. al.

The better performance of the present method is expected since the present method is more accurate that surface wave's effects are also incorporated in the analysis. The small discrepancies of the impedance levels at resonance may be accounted by the fact that the dielectric is assumed to be lossless in the present method that results in a larger Q-factor than the measured one.

Figures 6 and 7 show the convergence check for the moment method solutions for both the thinner and the thicker substrate. The solutions are shown to converge very fast, minor frequency shift is observed, and the percentage error between one mode and five modes are 0.4% and 0.8% respectively.

However, it is found that the single mode solution is closest to the measurement, it may be because the single mode current expansion is very close to the actual current distribution that addition of expansion modes will not give better approximation of the actual current distribution, but instead degrade it.

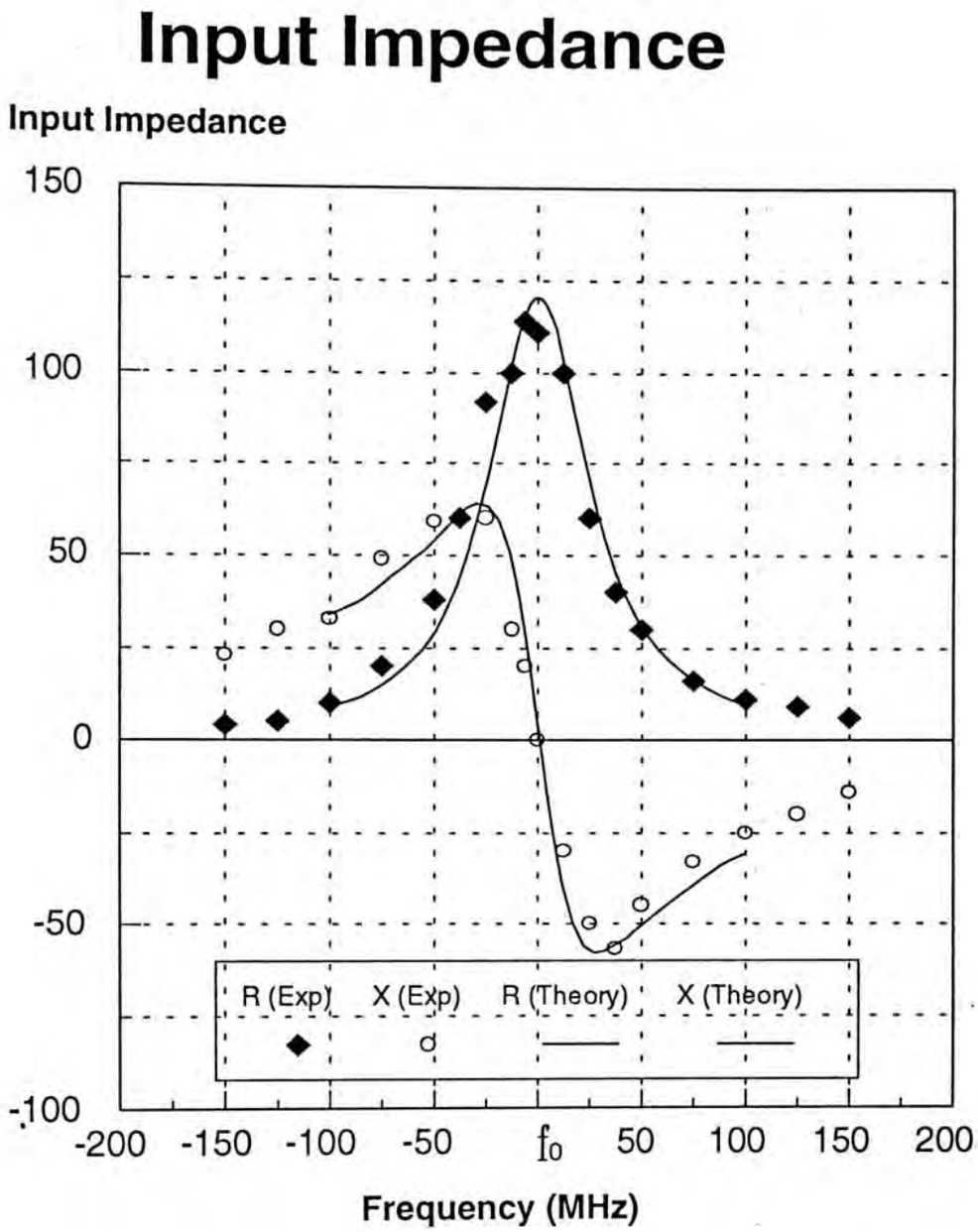

Figure 4 : Calculated and measured input impedance of TE_{01} mode [4] [5] as a function of deviation from resonant frequency. Calculated f_0 = 3.201 GHz, Measured f_0 = 3.170 GHz. a = 5 cm, h = b - a = 0.0795 cm, W = 4 cm, L = 3 cm, z' = -0.01 m, ε_r = 2.32.

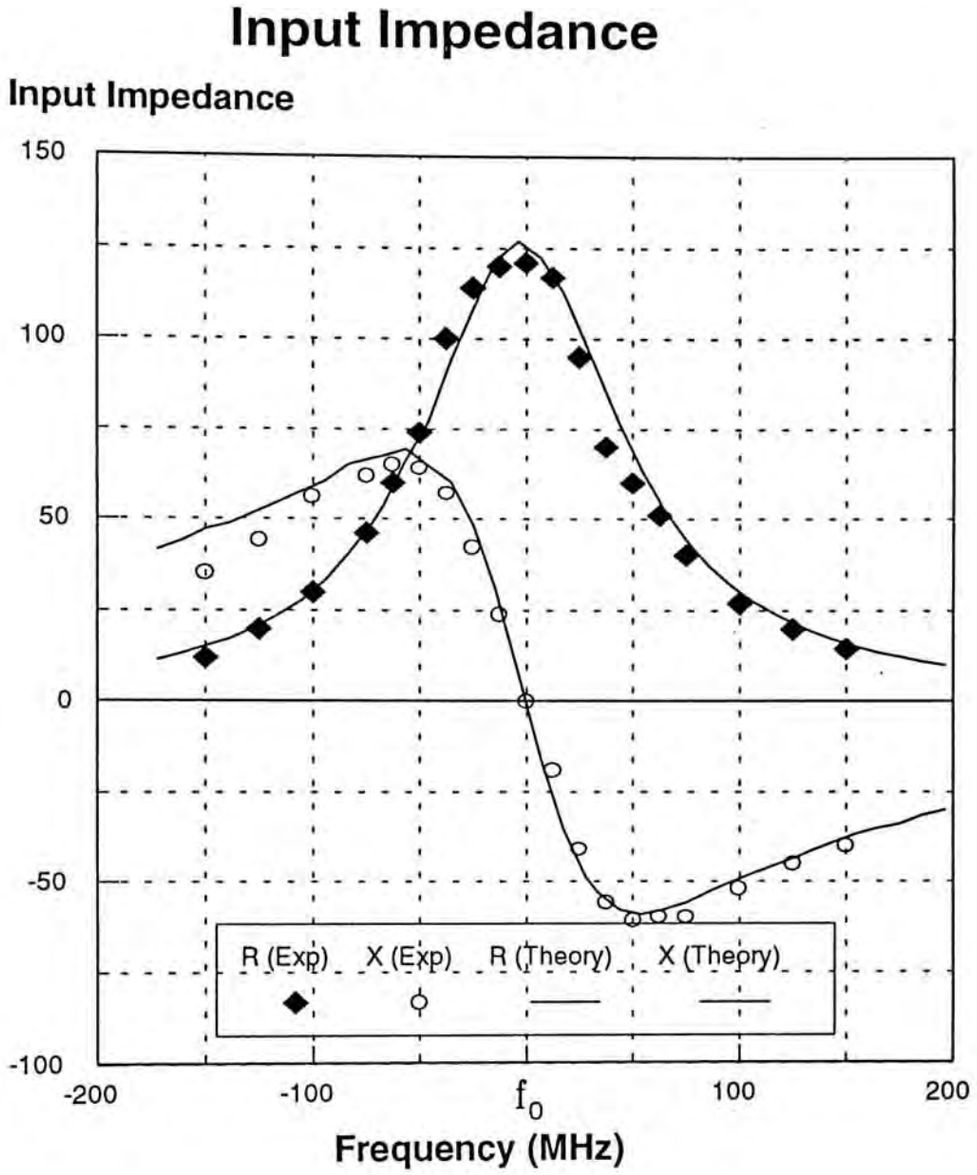

Figure 5 : Calculated and measured input impedance of TE_{01} mode [4] [5] as a function of deviation from resonant frequency. Calculated f_0 = 3.141 GHz, Measured f_0 = 3.135 GHz. a = 5 cm, h = b - a = 0.159cm, W = 4 cm, L = 3 cm, z' = -0.01m, ε_r = 2.32.

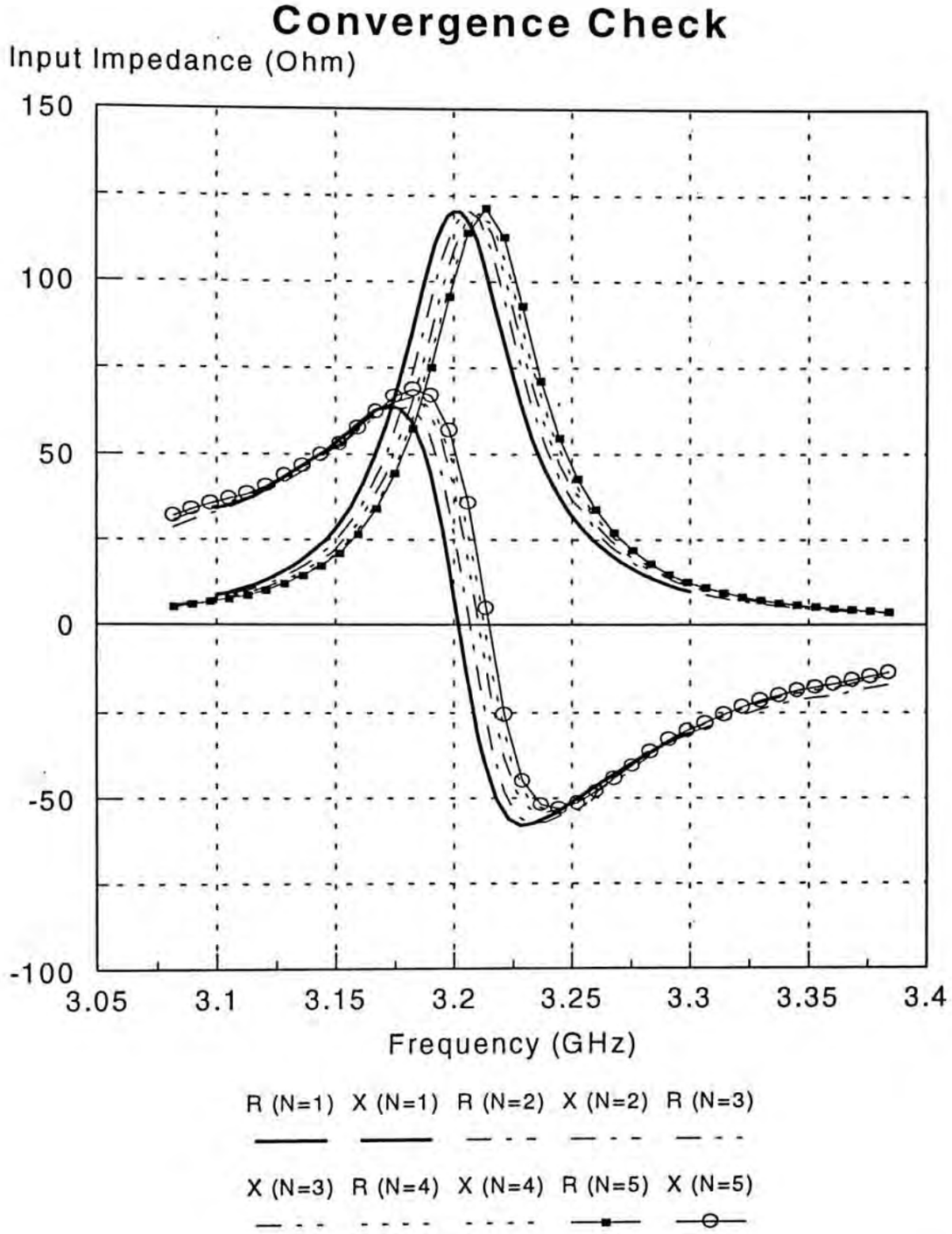

Figure 6 : Convergence check of the Moment method solution for the thinner substrate

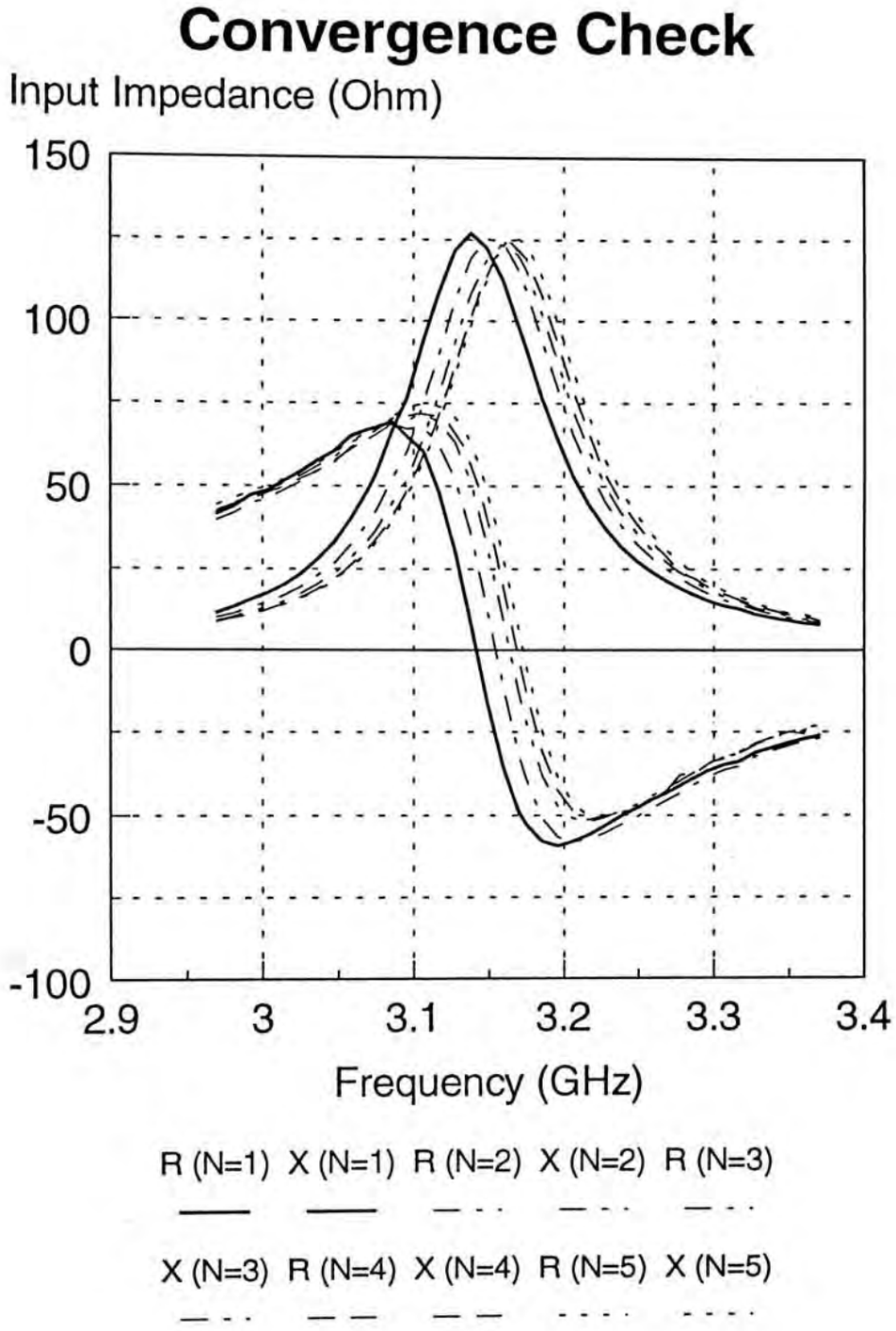

Figure 7 : Convergence check of the Moment method solution for the thicker substrate

4. REFERENCES

1. C.M. Krowne, "Cylindrical-rectangular microstrip antenna", *IEEE Trans. Antennas Propagat.* AP-31, pp. 194-199, 1983.

2. S. Fonseca and A. Giarola, "Analysis of microstrip wraparound antennas suing dyadic Green's functions", *IEEE Trans. Antennas Propagat.*, Vol. AP-31, pp. 248-253, Mar. 1983.

3. J. Ashkenazy, S. Shtrikman, and D. Treves, "Electric Surface Current Model for the Analysis of Microstrip Antennas on Cylindrical Bodies", *IEEE Trans. Antennas Propagat.*, Vol. AP-33, No. 3, March 1985.

4. K.M. Luk, K.F. Lee and J.S. Dahele, "Analysis of the Cylindrical-rectangular patch antenna", *IEEE Trans. Antennas Propagat.*, vol. 37, No. 2, Feb 1989.

5. J.S. Dahele, K.M. Luk, K.F. Lee and R.J. Mitchell, "Theoretical and experimental studies of the cylindrical-rectangular microstrip patch antenna", *Int. J. Electronics*, Vol. 68, No. 3, pp431-438, 1990.

6. J.S. Dahele, R.J. Mitchell, K.M. Luk and K.F. Lee, "Effect of curvature on characteristics of rectangular patch antenna", *Electronics Letters*, Vol. 23, No. 14, July 1987.

7. R.F. Harrington, *Time-harmonic electromagnetic fields*, McGraw-Hill 1961.

8. S.M. Ali, T.M. Habashy, J.F. Kiang and J.A. Kong, "Resonance in cylindrical-rectangular and wraparound microstrip structures", *IEEE Trans. Microwave Theory Tech.*, Vol. 37, No. 11, Nov 1989.

9. T.M. Habashy, S.M. Ali, and J.A. Kong, "Input impedance and radiation pattern if cylindrical-rectangular and wraparound microstrip antennas", *IEEE Trans. Antennas Propagat.* Vol. 38, No. 5, pp. 722-731, May 1990.

10. D.M. Pozar, "Input impedance and mutual coupling of rectangular microstrip antennas", *IEEE Trans. Antennas Propagat.*, Vol. AP-30, No. 6, pp. 1191-1196, Nov. 1982.

CHAPTER 4

MUTUAL IMPEDANCE OF CYLINDRICAL-RECTANGULAR MICROSTRIP PATCH ANTENNAS

1. INTRODUCTION

Microstrip antenna arrays have found wide application in recent years out of their many unique and attractive properties, to name a few, low in profile, light in weight, compact and comformable in structure. Similarly it is also desirable to build microstrip antenna arrays on curved surface, and circular cylinder is one of the simplest curved structure. The mutual coupling between microstrip antennas is an important criterion in antenna array design, since the coupling effects may produce increased sidelobe levels, main beam squint and array blindness at some scan angles.

In this chapter, a method for calculating mutual coupling between cylindrical-rectangular microstrip antennas is developed.

2. FORMULATION

Consider the configurations as shown in figures 1 and 2, two microstrip patch antennas are assumed to be identical both geometrically and in the feed positions. The dimensions of the patch antenna is W by L cm, where $W=2b\phi_0$.

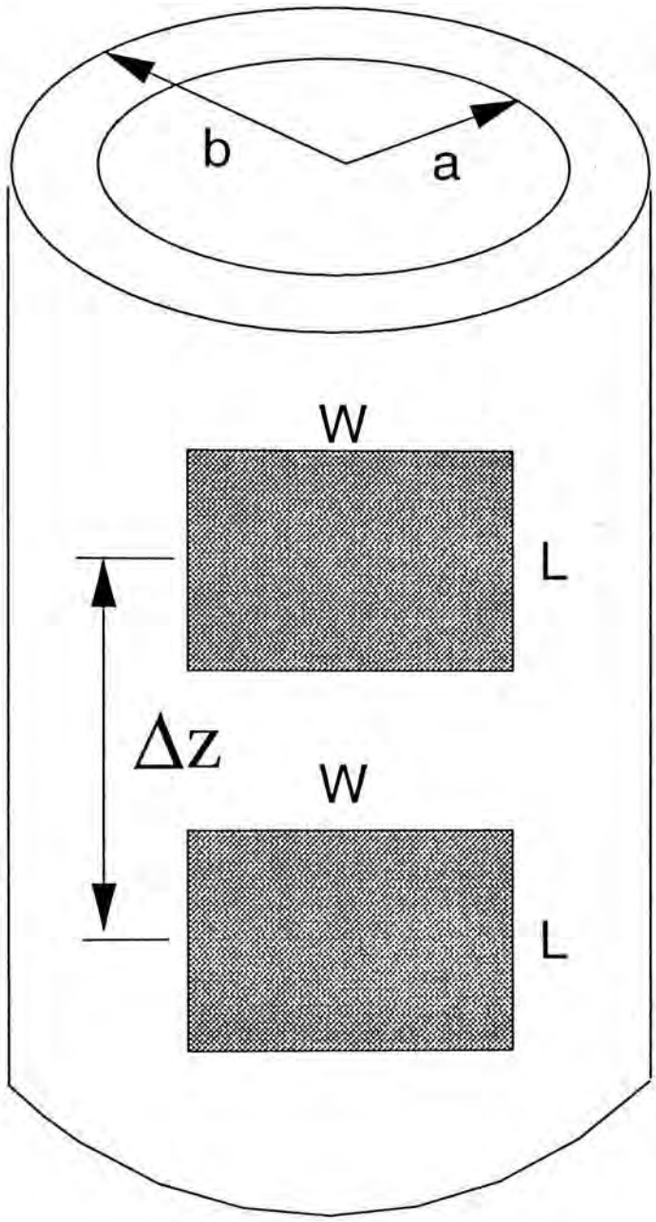

Figure 1 : E-plane coupling

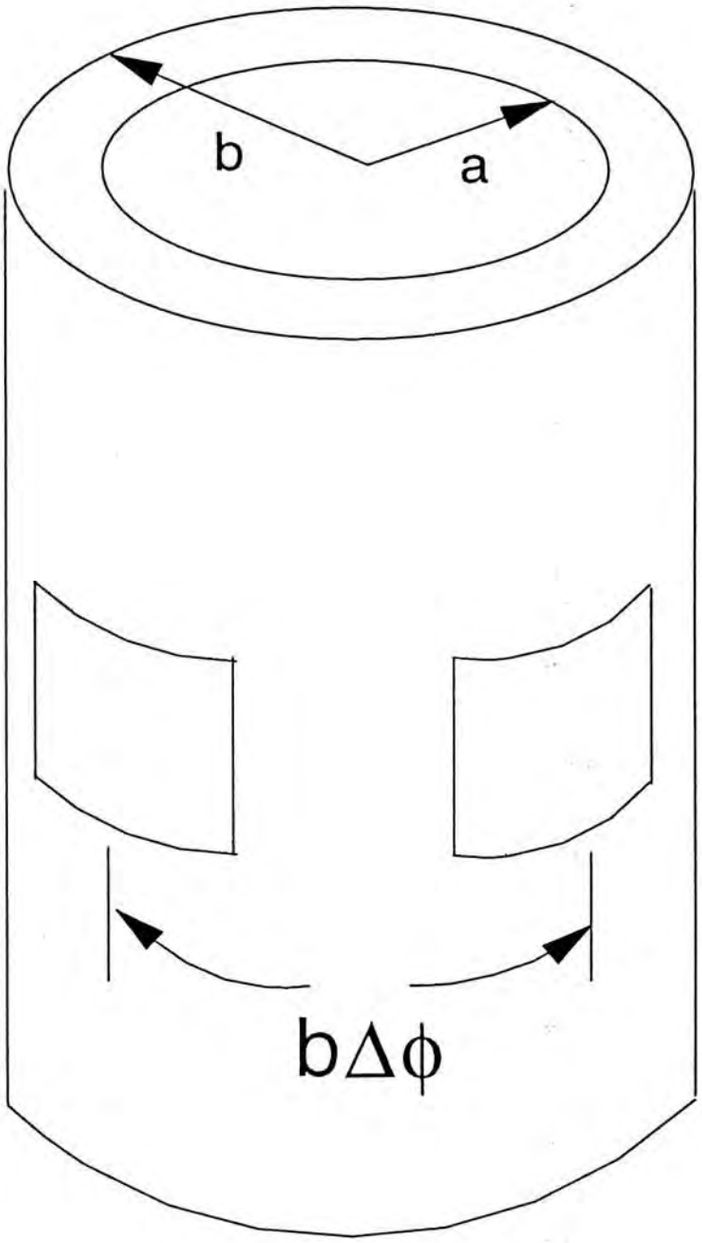

Figure 2 : H-Plane Coupling

Consider the two-port model (figure 3) of the two element microstrip antenna configuration.

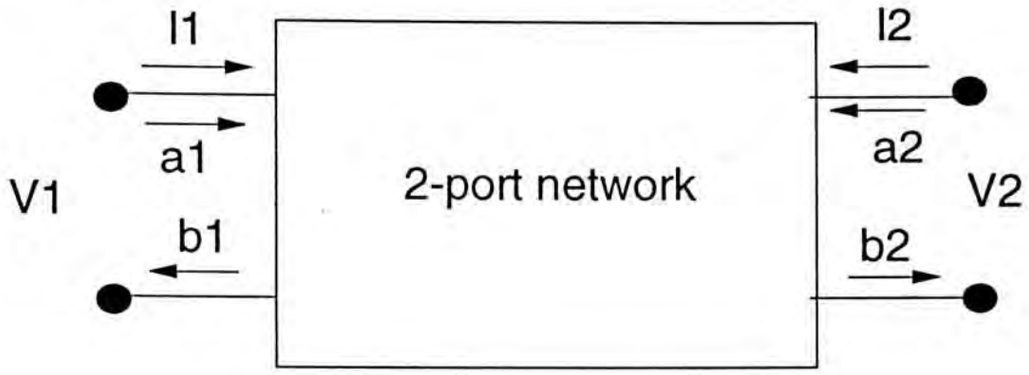

Figure 3 :Two-port model

The relationship between the port voltages and port currents are :

$$\begin{bmatrix} V_1^P \\ V_2^P \end{bmatrix} = \begin{bmatrix} Z_{11}^P & Z_{12}^P \\ Z_{21}^P & Z_{22}^P \end{bmatrix} \begin{bmatrix} I_1^P \\ I_2^P \end{bmatrix} \qquad (4.1)$$

$$Z_{11}^P = \frac{-\iiint_V \bar{E}^{(1)} \cdot \bar{J}_i^{(1)} dv}{(I_i)^2}$$

$$Z_{12}^P = \frac{-\iiint_V \bar{E}^{(1)} \cdot \bar{J}_i^{(2)} dv}{(I_i)^2}$$

$$Z_{21}^P = \frac{-\iiint_V \bar{E}^{(2)} \cdot \bar{J}_i^{(1)} dv}{(I_i)^2}$$

$$Z_{22}^P = \frac{-\iiint_V \bar{E}^{(2)} \cdot \bar{J}_i^{(2)} dv}{(I_i)^2}$$

where

Z_{11}^{P} is the input impedance of port 1 with port 2 open-circuited.

Z_{22}^{P} is the input impedance of port 2 with port 1 open-circuited.

Z_{12}^{P}, Z_{21}^{P} are the open-circuit transfer impedance between the two ports.

$\overline{E}^{(1)}$ is the total electric field due to $\overline{J}_i^{(1)}$ which is the source current distribution at port 1.

$\overline{E}^{(2)}$ is the total electric field due to $\overline{J}_i^{(2)}$ which is the source current distribution at port 2.

I_i is the i-th terminal current from the source.

Unless the two patches are very close to each other, the influence of the other patch to the surface current distribution is negligible that we can consider the surface current distribution is similar to that of a single patch configuration.

Hence, the analysis of the mutual impedance between two microstrip patch antennas on a metallic cylinder can start from equation (3.20) of the previous chapter.

The mutual impedance between two identical microstrip antennas are :

$$Z_{21} = \frac{-\iiint_V \bar{E}^{(2)} \cdot \bar{J}_i^{(1)} dv}{(I_i)^2} \qquad (4.1)$$

where the superscripts (1) and (2) indicate the port 1 and port 2 respectively. Because of reciprocity, $Z_{12} = Z_{21}$, so we have,

$$\begin{aligned} Z_{12} &= \frac{-\iiint_V \bar{E}^{(1)} \cdot \bar{J}_i^{(2)} dv}{(I_i)^2} \\ &= -\iiint_V \bar{E}^{(1)} \cdot \bar{J}_i^{(2)} dv \qquad \because I_i = 1A \\ &= -\iiint_V \left[\sum_{p=1}^{N_z} I_{zp} \bar{E}_{zp}^{(1)} + \sum_{q=1}^{N_\phi} I_{\phi q} \bar{E}_{\phi q}^{(1)} \right] \cdot \bar{J}_i^{(2)} dv \\ &= -\sum_{p=1}^{N_z} I_{zp} \left[\iiint_V \bar{E}_{zp}^{(1)} \cdot \bar{J}_i^{(2)} dv \right] - \sum_{q=1}^{N_\phi} I_{\phi q} \left[\iiint_V \bar{E}_{\phi q}^{(1)} \cdot \bar{J}_i^{(2)} dv \right] \\ &= -\sum_{p=1}^{N_z} I_{zp} V_{zp}^{(2)} - \sum_{q=1}^{N_\phi} I_{\phi q} V_{\phi q}^{(2)} \end{aligned} \qquad (4.2)$$

where

$$V_{zp}^{(2)} = \iiint_V \bar{E}_{zp}^{(1)} \cdot \bar{J}_i^{(2)} dv \qquad (4.3a)$$

$$V_{\phi q}^{(2)} = \iiint_V \bar{E}_{\phi q}^{(1)} \cdot \bar{J}_i^{(2)} dv \qquad (4.3b)$$

Assuming the probe-fed current be modeled by a delta-function located at the feed-point. The equations (4.3a) and (4.3b) can be simplified to the following form :

$$V_{zp}^{(2)} = \int_a^b \int_0^{2\pi} \int_{-\infty}^{\infty} \frac{1}{\rho}\delta(\phi-\phi_s-\Delta\phi)\delta(z-z_s-\Delta z)\frac{1}{2\pi}\sum_{n=-\infty}^{\infty}\int_{-\infty}^{\infty}\tilde{G}_{\rho z}\tilde{J}_{zp}(n,k_z)e^{j(n\phi_s-k_z z_s)}dk_z\rho d\rho d\theta dz$$

$$= \frac{1}{2\pi}\int_a^b \int_{-\infty}^{\infty}\sum_{n=-\infty}^{\infty}\tilde{G}_{\rho z}\tilde{J}_{zp}(n,k_z)e^{j(n\phi_s+\Delta\phi)}e^{-j(k_z z_s+\Delta z)}d\rho dk_z \qquad (4.4a)$$

$$V_{\phi q}^{(2)} = \int_a^b \int_0^{2\pi} \int_{-\infty}^{\infty} \frac{1}{\rho}\delta(\phi-\phi_s-\Delta\phi)\delta(z-z_s-\Delta z)\frac{1}{2\pi}\sum_{n=-\infty}^{\infty}\int_{-\infty}^{\infty}\tilde{G}_{\rho\phi}\tilde{J}_{\phi q}(n,k_z)e^{j(n\phi_s-k_z z_s)}dk_z\rho d\rho d\theta dz$$

$$= \frac{1}{2\pi}\int_a^b \int_{-\infty}^{\infty}\sum_{n=-\infty}^{\infty}\tilde{G}_{\rho\phi}\tilde{J}_{\phi q}(n,k_z)e^{j(n\phi_s+\Delta\phi)}e^{-j(k_z z_s+\Delta z)}d\rho dk_z \qquad (4.4b)$$

We choose the sinusoidal function as the entire domain basis functions, and also assume the current distribution is a separable function of z and ϕ.

$$\bar{J}_s = \hat{z}\sum_{p=1}^{N_z} I_{zp}J_{zp} + \hat{\phi}\sum_{q=1}^{N_\phi} I_{\phi q}J_{\phi q} \qquad (4.5)$$

where

$$J_{zp} = \sin\left[\frac{2p-1}{L}\left(z-\frac{L}{2}\right)\pi\right]$$

$$J_{\phi q} = \sin\left[\frac{2q-1}{2\phi_0}(\phi-\phi_0)\pi\right]$$

Then, the transformed current components are shown as follows :

$$\underline{\tilde{J}_s} = \hat{z}\sum_{p=1}^{N_z} I_{zp}\tilde{J}_{zp} + \hat{\phi}\sum_{q=1}^{N_\phi} I_{\phi q}\tilde{J}_{\phi q} \qquad (4.6)$$

where

$$\tilde{J}_{zp}(n,k_z) = \int_0^{2\pi}\int_{-\infty}^{\infty} J_{zp}(\phi,z)e^{-j(n\phi-k_z z)}d\phi dz$$

$$= 4\pi L\phi_0 \sin c(n\phi_0)\frac{r\cos\left(\frac{k_z L}{2}\right)}{(r\pi)^2-(k_z L)^2}$$

$$\tilde{J}_{\phi q}(n,k_z) = \int_0^{2\pi}\int_{-\infty}^{\infty} J_{\phi q}(\phi,z)e^{-j(n\phi-k_z z)}d\phi dz$$

$$= 4\pi L\phi_0 \sin c\left(\frac{k_z L}{2}\right)\frac{s\cos(n\phi_0)}{(s\pi)^2-(n\phi_0)^2}$$

$$r = 2p - 1$$

$$s = 2q - 1$$

3. DISCUSSION

From figures 4 and 5, we can observe the trend that E-plane coupling is larger than the H-plane coupling, this is consistent with mutual coupling analysis on planar microstrip antennas.

It is shown in the figures that both the E-plane and H-plane coupling drop approximately monotonically as the separation between the facing edges increases. Since the mutual coupling is caused by the simultaneous effects of interaction through the space radiation, and interaction through the surface waves, and the surface wave coupling decays more slowly than the space wave coupling, the decay of coupling as separation increases is mainly due to weakened space wave interaction.

Figure 6 shows the effects of varying the substrate thickness on the mutual coupling. It is seen that the mutual impedance has larger values over various edge separations for a thicker substrate. It is because the surface wave coupling increases rapidly with the substrate thickness as in the planar case.

Figure 7 shows the effects of varying the relative permittivity of the substrate on the mutual coupling. The mutual coupling is found to decrease for using substrate of larger relative permittivity. Although increasing the relative permittivity of the substrate will excite stronger surface waves thus increasing the surface wave coupling, a substrate with high relative

permittivity will trap the waves or energy more tightly inside the dielectric substrate that the space wave radiation and hence the space-wave coupling is weakened, the overall effect is reduced mutual coupling which also indicates that the space-wave coupling is much stronger than the surface wave coupling (that justify the neglecting of surface wave effects in some approximate analysis of mutual coupling).

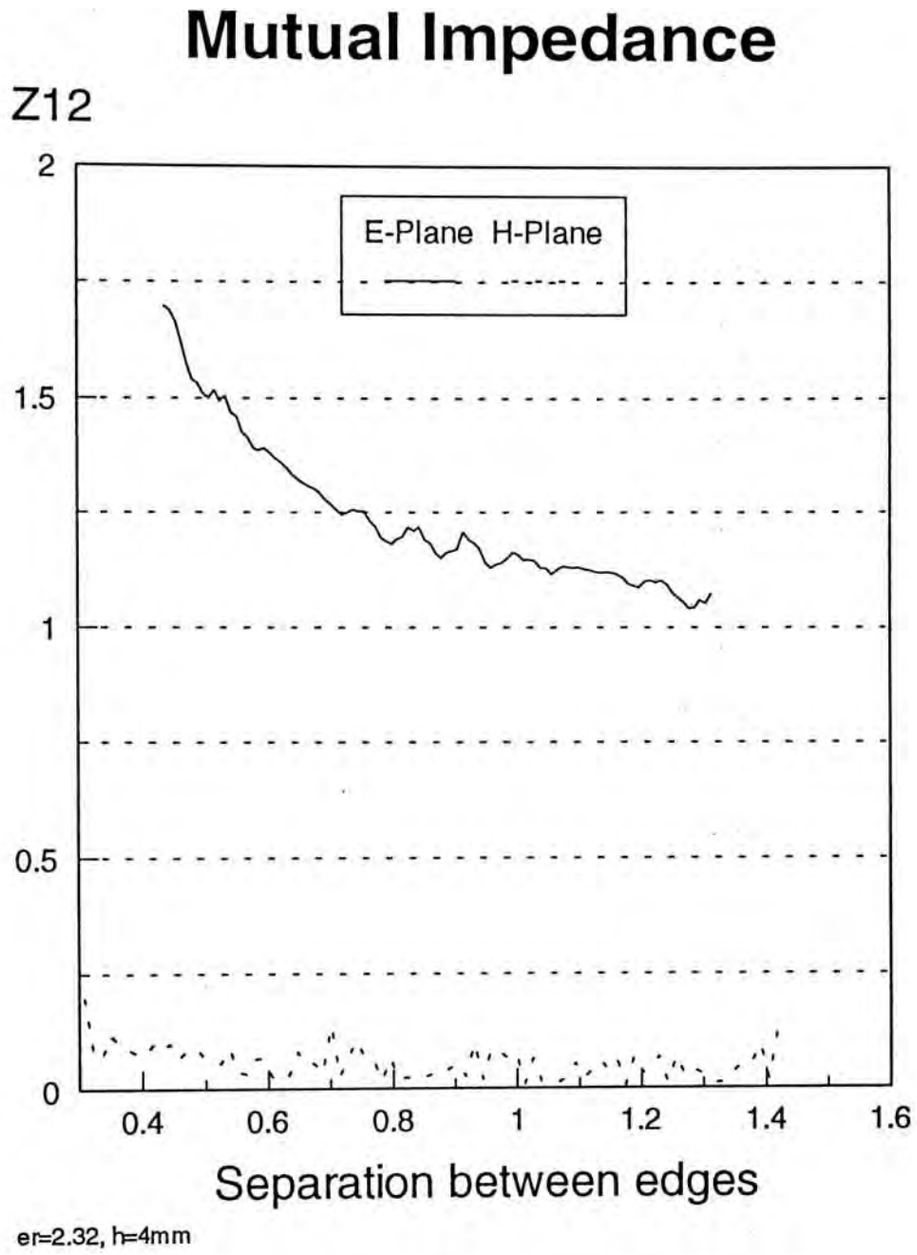

Figure 4 : Mutual Impedance (E-plane and H-plane) against separations between the edges.

W = 4.0 cm, L = 3.0 cm, a = 5.0 cm, b-a = 4.0 mm, ε_r = 2.32, z' = -0.01m

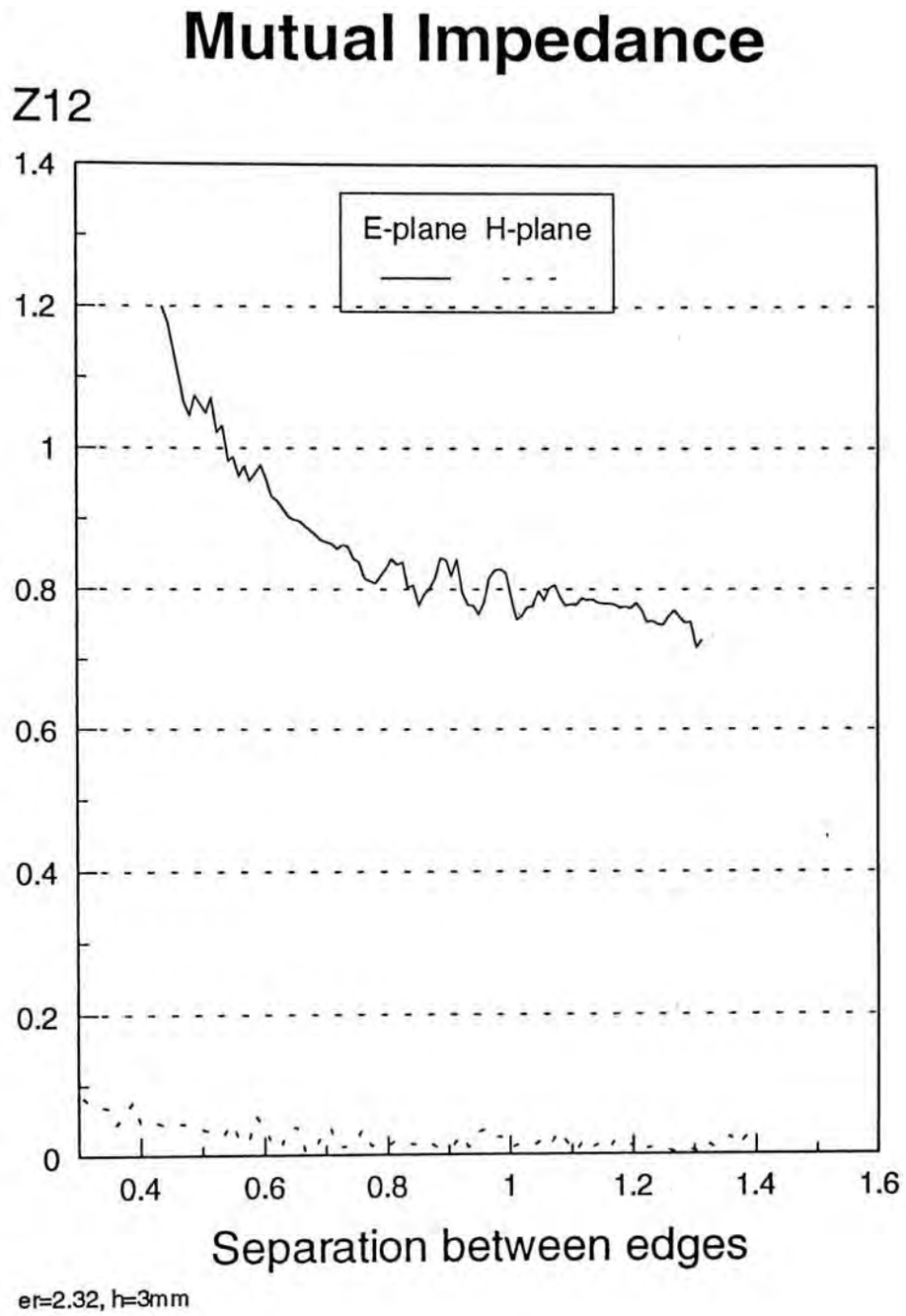

Figure 5 : Mutual Impedance (E-plane and H-plane) against separations between the edges.

W = 4.0 cm, L = 3.0 cm, a = 5.0 cm, b-a = 3.0 mm, ε_r = 2.32, z' = -0.01m

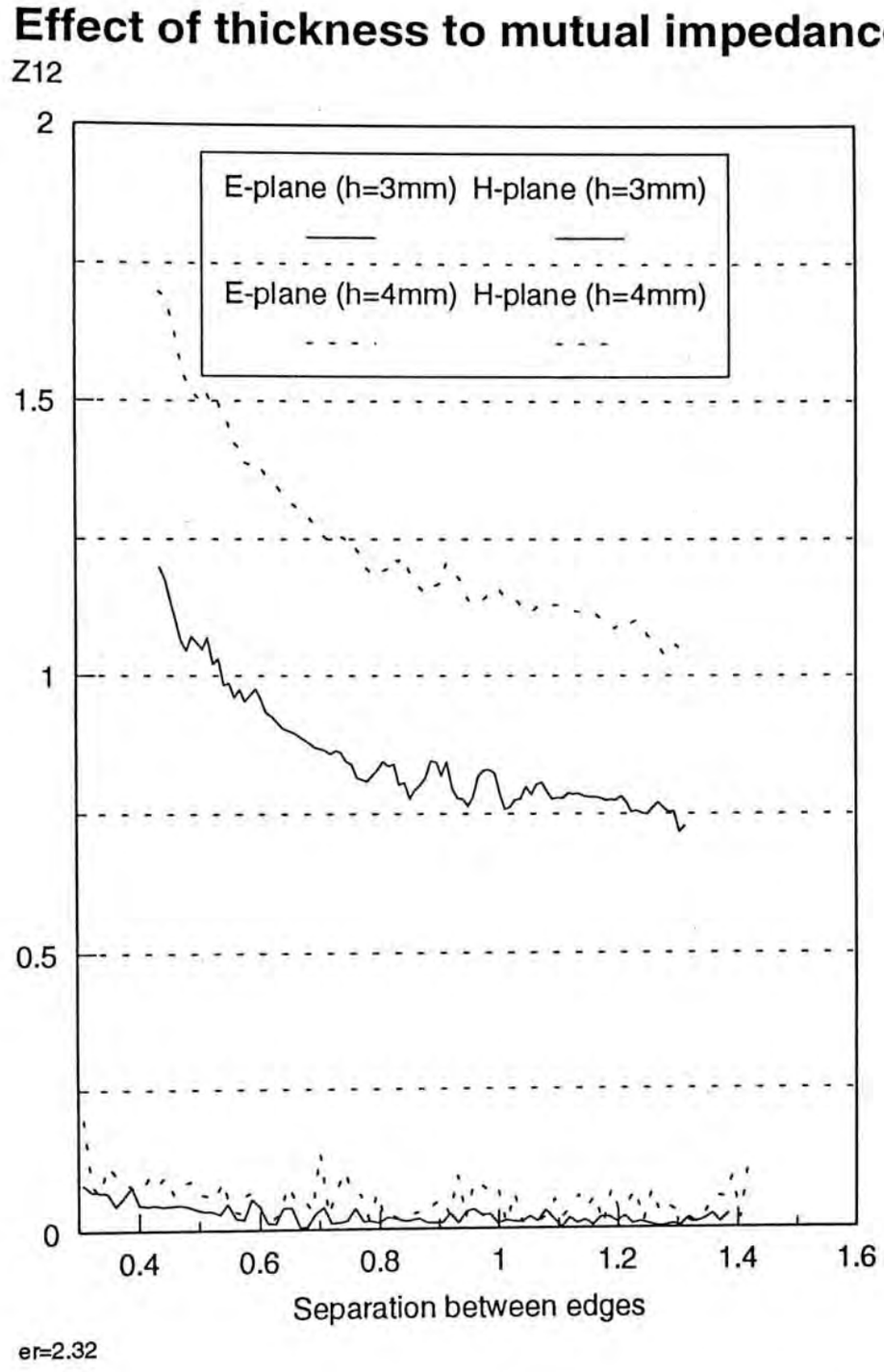

Figure 6 : Effects of variation of substrate thickness to mutual impedance

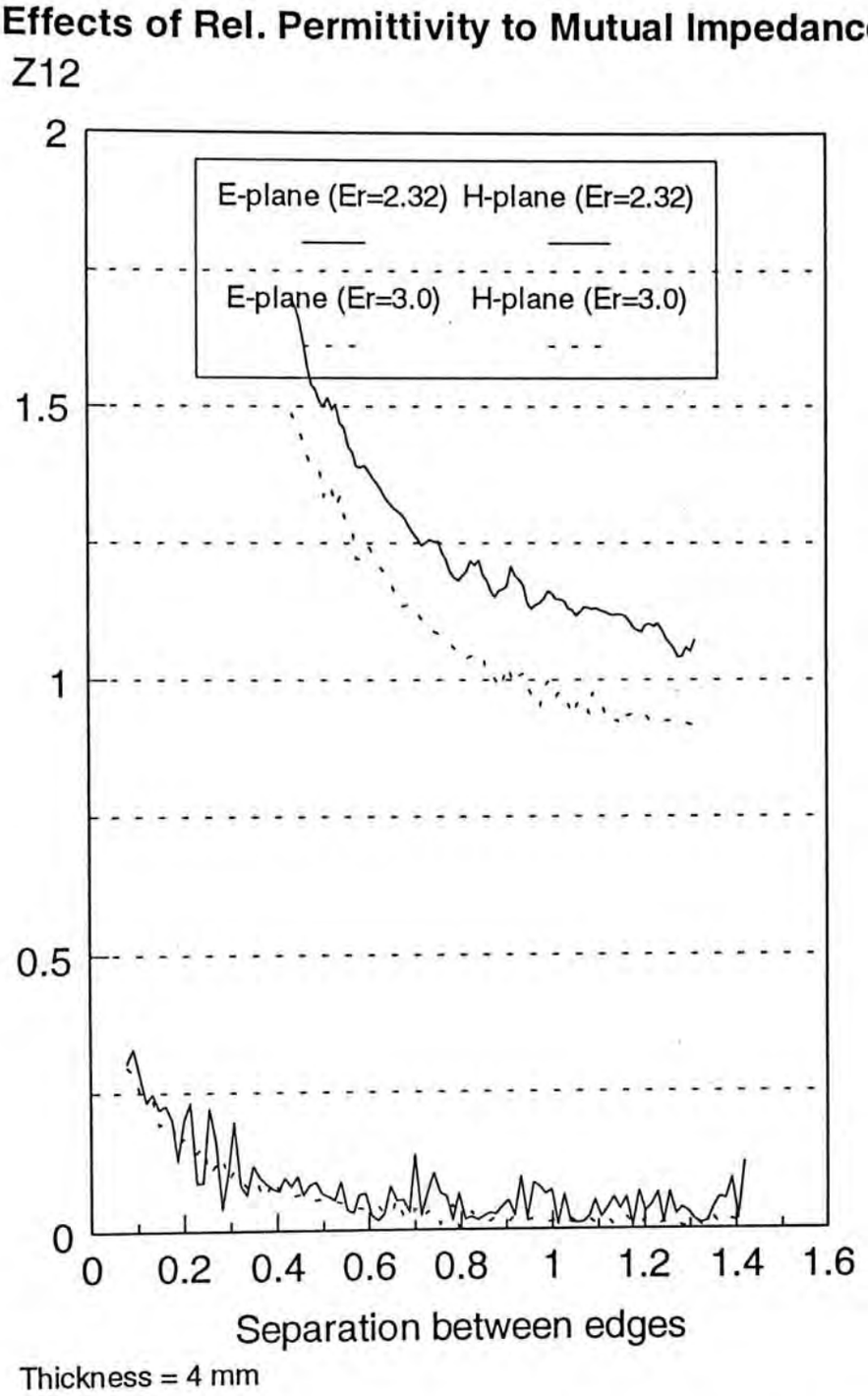

Figure 7 : Effects of variation of rel. permittivity to mutual impedance

4. REFERENCES

1. R.P. Jedlicka, M.T. Poe, and K.R. Carver, "Measured mutual coupling between microstrip antennas", *IEEE Trans. Antennas Propagat.*, Vol. AP-29, pp. 147-149. Jan. 1981.

2. E. Penard, and J.P. Daniel, "Mutual coupling between microstrip antennas", *Electron. Lett.*, Vol. 18, no. 14, pp. 605-607, July 1982.

3. E.H. Van Lil, and A.R. Van De Capelle, "Transmission line model for mutual coupling between microstrip antennas", *IEEE Trans. Antennas Propagat.*,

4. D.M. Pozar, "Input impedance and mutual coupling of rectangular microstrip antennas", *IEEE Trans. Antennas Propagat.*, Vol. AP-30, No. 6, pp. 1191-1196, Nov. 1982.

5. K.C. Gupta, and A. Benalla, *Microstrip Antenna Design*, Artech House, 1988.

CHAPTER 5

RESONANCE OF RECTANGULAR MICROSTRIP ANTENNA INSIDE A METALLIC CYLINDER

1. INTRODUCTION

From this chapter onwards, a study of microstrip antennas wrapped onto the inner surface of a metallic cylinder will be discussed.

Microstrip antennas have possible applications as focusing antenna for hyperthermia treatment. However, the physicians together with the patient are exposed to microwave radiation, which may be hazardous out of prolonged microwave exposure. This possible hazard can be avoided by building the focusing antenna inside a metallic cylinder where the patient can have the treatment.

In the design of microstrip antennas, it is of great importance to determine accurately the resonant frequencies of the antenna out of its narrow bandwidth. The resonant frequencies of a planar microstrip patch have been studied extensively [1]-[6], while the resonant frequencies of cylindrical-rectangular microstrip patch had been studied using cavity model [7] and integral equations method [8]. However, the resonance of a microstrip patch mounted inside a hollow metallic cylinder remains unreported.

In this chapter, we rigorously analyze the resonance of the microstrip patch mentioned above. The radiator is replaced by a surface current distribution on the interface between air and dielectric. The formulation will lead to a set of integral equations from which the current distribution on the patch can be evaluated. The set of integral equations is solved using Galerkin's method with sinusoidal basis functions. Muller's method is then used to locate the zero of the eigenvalue equation whose root is the complex resonant frequency. Both the real and the imaginary part of the complex resonant frequencies will be calculated with various dielectric substrate thicknesses. The resonance of TE_{01} mode is studied

2. FORMULATION

Figures 1 and 2 show the geometry of the problem. An infinitely long hollow metallic cylinder of inner radius a is coated upon it's inner surface a layer of dielectric substrate whose thickness is t, relative permittivity ε_r, and relative permeability μ_0. A metallic patch, whose dimensions are L $\times$ W ($W = 2b\phi_0$), is printed on the surface of the dielectric substrate. Both the patch and the hollow metallic cylinder are assumed to be perfectly conducting. The time convention $e^{j\omega t}$ is used. In figure 1, region 1 is the region inside the dielectric substrate while region 2 is the free space within the cylinder.

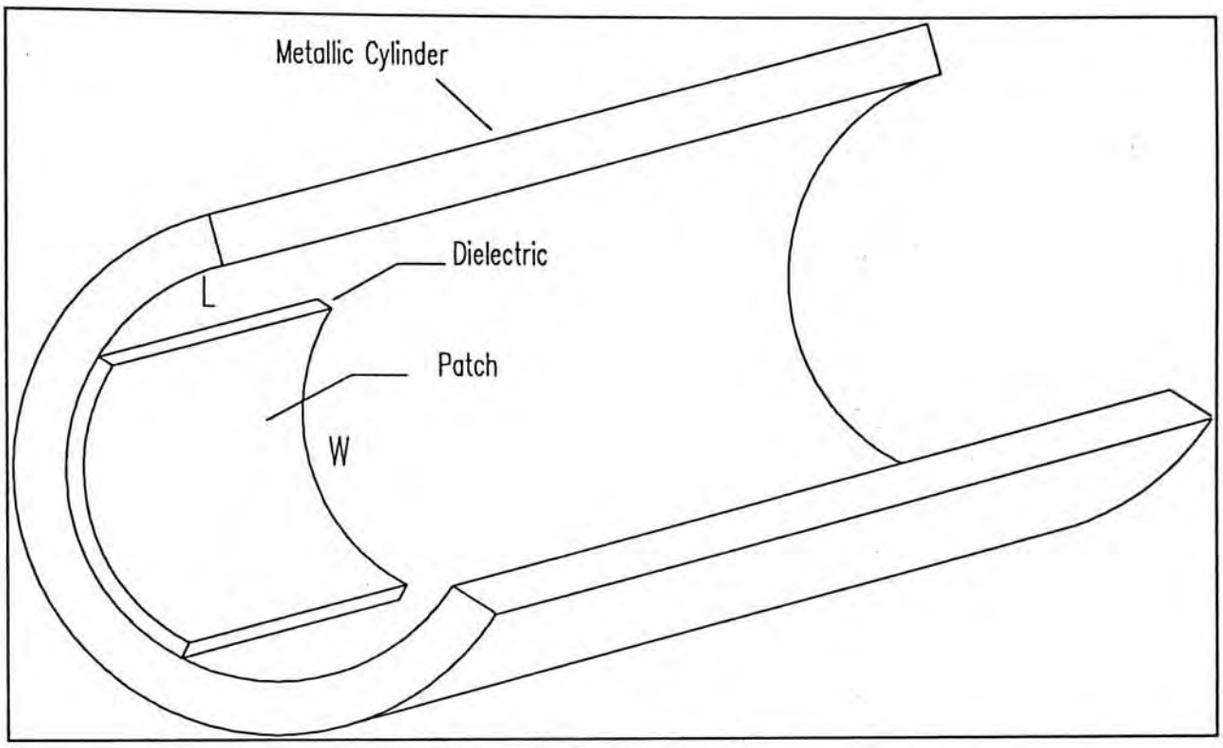

Figure 1 : The antenna configuration

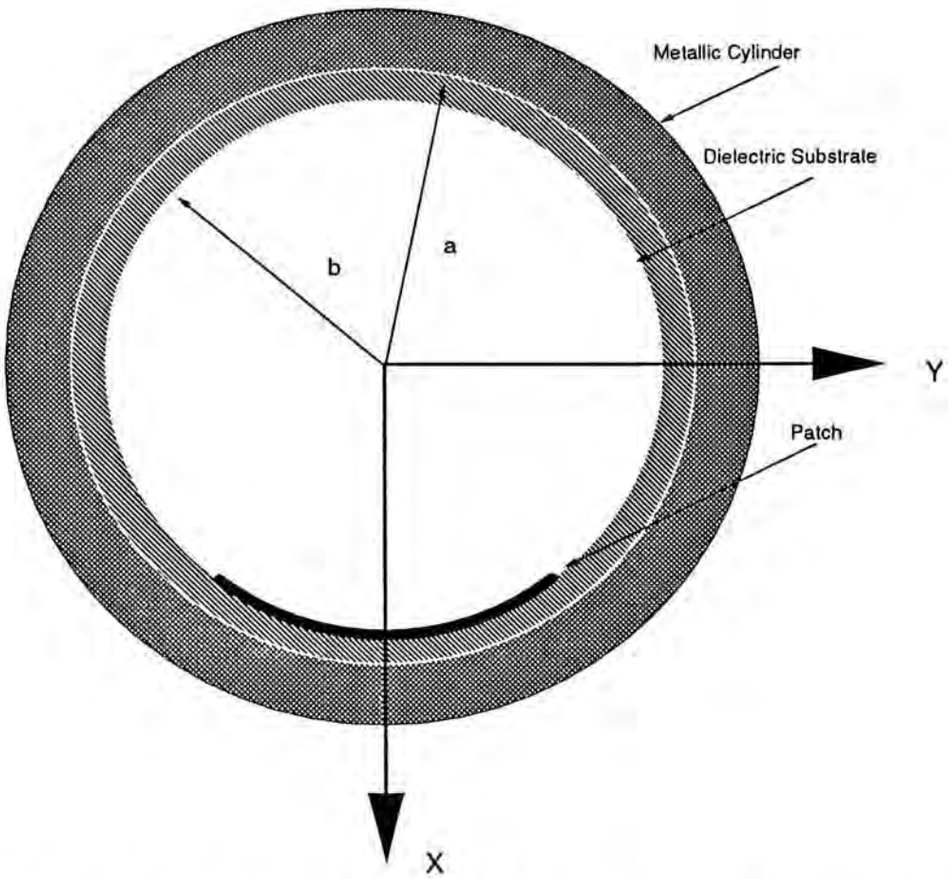

Figure 2 : Cross-sectional View of the antenna configuration

For TM and TE decomposition of waves, we have :

$$\overline{A} = \Psi_m \hat{z}, \quad \overline{F} = 0 \quad (TM_z)$$
$$\overline{A} = 0, \quad \overline{F} = \Psi_e \hat{z} \quad (TE_z)$$

Hence we arrive at a set of scalar wave equations as follows :

$$\nabla^2 \begin{Bmatrix} \Psi_{mi} \\ \Psi_{ei} \end{Bmatrix} + k_i^2 \begin{Bmatrix} \Psi_{mi} \\ \Psi_{ei} \end{Bmatrix} = 0 \quad i = 1,2 \qquad (5.1)$$

where $k_1^2 = \varepsilon_r k_0^2$, and $k_2^2 = k_0^2$. The subscript i is used to denote region 1 or 2. A Fourier-Series-Fourier-Transform pair is defined similar to that of Ashkenazy et. al. [9] :

$$A(\rho,\phi,z) = \frac{1}{2\pi} \sum_{n=-\infty}^{\infty} \int_{-\infty}^{\infty} \tilde{A}(\rho,n,k_z) e^{j(n\phi - k_z z)} dk_z$$

$$\tilde{A}(\rho,n,k_z) = \frac{1}{2\pi} \int_0^{2\pi} \int_{-\infty}^{\infty} A(\rho,\phi,z) e^{-j(n\phi - k_z z)} dz d\phi \qquad (5.2)$$

The scalar wave equations are then expressed in cylindrical coordinate system and transformed using (5.2), the wave equations have the form of a Bessel differential equation :

$$\frac{d^2\tilde{\Psi}_{mi}}{d\rho^2} + \frac{1}{\rho}\frac{d\tilde{\Psi}_{mi}}{d\rho} + \left(k_{\rho i}^2 - \frac{n^2}{\rho^2}\right)\tilde{\Psi}_{mi} = 0$$

$$\frac{d^2\tilde{\Psi}_{ei}}{d\rho^2} + \frac{1}{\rho}\frac{d\tilde{\Psi}_{ei}}{d\rho} + \left(k_{\rho i}^2 - \frac{n^2}{\rho^2}\right)\tilde{\Psi}_{ei} = 0 \qquad (5.3)$$

where $k_{\rho i}^2 = k_i^2 - k_z^2$, i = 1, 2.

The solutions of the transformed wave equations in the 2 regions are :

Region 1:

$$\tilde{\Psi}_{m1}(\rho,n,k_z) = A_m(n,k_z)J_n(k_{\rho 1}\rho) + B_m(n,k_z)Y_n(k_{\rho 1}\rho)$$

$$\tilde{\Psi}_{e1}(\rho,n,k_z) = A_e(n,k_z)J_n(k_{\rho 1}\rho) + B_e(n,k_z)Y_n(k_{\rho 1}\rho) \quad (5.4)$$

Region 2:

$$\tilde{\Psi}_{m2}(\rho,n,k_z) = C_m(n,k_z)J_n(k_{\rho 2}\rho)$$

$$\tilde{\Psi}_{e2}(\rho,n,k_z) = C_e(n,k_z)J_n(k_{\rho 2}\rho) \quad (5.5)$$

We can always express the field components in terms of the vector electric potential and vector magnetic potential [10], and we can employ the boundary conditions to eliminate the coefficients. By matching the boundary conditions on the tangential components of electric fields (E_z, E_ϕ) at the surface of the cylinder which is assumed to be perfectly conducting, we obtain the following relationships between the spectral amplitudes A_m and B_m, A_e and B_e :

$$\alpha_m = -\frac{B_m}{A_m} = \frac{J_n(k_{\rho 1}a)}{Y_n(k_{\rho 1}a)}$$

$$\alpha_e = -\frac{B_e}{A_e} = \frac{J_n'(k_{\rho 1}a)}{Y_n'(k_{\rho 1}a)} \quad (5.6)$$

Similarly by matching the boundary conditions on the tangential components of electric fields at the patch's surface, we obtain the followings :

$$A_m = \beta_m C_m$$
$$A_e = \gamma_m C_m + \gamma_e C_e \qquad (5.7)$$

where

$$\beta_m = \left(\frac{k_{\rho 2}}{k_{\rho 1}}\right)^2 \varepsilon_r \frac{J_n(k_{\rho 2} b)}{T_m(b)}$$

$$\gamma_m = \frac{k_0^2(\varepsilon_r - 1)}{j\omega\varepsilon_0 b} \cdot \frac{n k_z}{k_{\rho 1}^2} \cdot \frac{J_n(k_{\rho 2} b)}{T_e'(b)}$$

$$\gamma_e = k_{\rho 2} \frac{J_n'(k_{\rho 2} b)}{T_e'(b)}$$

$$T_m(b) = J_n(k_{\rho 1} b) - \alpha_m Y_n(k_{\rho 1} b)$$

$$T_e'(b) = k_{\rho 1}\left[J_n'(k_{\rho 1} b) - \alpha_e Y_n'(k_{\rho 1} b)\right]$$

An expression relating the current on the patch to the spectral amplitudes is to be derived next. It can be achieved by matching the discontinuity in the tangential components of the magnetic field to the surface current distribution. The following expression is found :

$$\begin{bmatrix} \tilde{J}_{sz}(b, n, k_z) \\ \tilde{J}_{s\phi}(b, n, k_z) \end{bmatrix} = \overline{\overline{M}} \begin{bmatrix} C_m \\ C_e \end{bmatrix} \qquad (5.8)$$

where $\tilde{J}_{s\phi}$ is the transformed ϕ-directed surface current, and $\tilde{J}_{sz}$ is the transformed z-directed surface current, and

$$\overline{\overline{M}} = \begin{bmatrix} M_{11} & M_{12} \\ M_{21} & M_{22} \end{bmatrix}$$

$$M_{11} = -k_{\rho 2} J_n'(k_{\rho 2} b) + \beta_m T_m'(b) - \frac{n k_z \gamma_m T_e(b)}{j\omega\mu_0 b}$$

$$M_{12} = \frac{-n k_z}{j\omega\mu_0 b}\left[-J_n(k_{\rho 2} b) + \gamma_e T_e(b)\right]$$

$$M_{21} = \frac{k_{\rho 1}^2}{j\omega\mu_0}\gamma_m T_e(b)$$

$$M_{22} = \frac{1}{j\omega\mu_0}\left[-k_{\rho 2}^2 J_n(k_{\rho 2} b) + k_{\rho 1}^2 \gamma_e T_e(b)\right]$$

The transformed tangential electric field components are shown to be related to the field spectral amplitudes as follows :

$$\begin{bmatrix} \tilde{E}_z(\rho, n, k_z) \\ \tilde{E}_\phi(\rho, n, k_z) \end{bmatrix} = \begin{bmatrix} T_{11} & T_{12} \\ T_{21} & T_{22} \end{bmatrix} \begin{bmatrix} C_m \\ C_e \end{bmatrix} \qquad (5.9)$$

where

$$T_{11} = \frac{k_{\rho 2}^2}{j\omega\varepsilon_0} J_n(k_{\rho 2} b)$$

$$T_{12} = 0$$

$$T_{21} = \frac{nk_z}{j\omega\varepsilon_0 b} J_n(k_{\rho 2} b)$$

$$T_{22} = k_{\rho 2} J_n'(k_{\rho 2} b)$$

From (5.8) and (5.9), we can obtain the relationship between the patch current distribution and the electric field on the patch in the spectral domain, and hence we can derive the spectral domain Green's function :

$$\begin{bmatrix} \tilde{E}_z(\rho, n, k_z) \\ \tilde{E}_\phi(\rho, n, k_z) \end{bmatrix} = \begin{bmatrix} \tilde{G}_{zz} & \tilde{G}_{z\phi} \\ \tilde{G}_{\phi z} & \tilde{G}_{\phi\phi} \end{bmatrix} \begin{bmatrix} \tilde{J}_{sz} \\ \tilde{J}_{s\phi} \end{bmatrix} \qquad (5.10)$$

where

$$\begin{bmatrix} \tilde{G}_{zz} & \tilde{G}_{z\phi} \\ \tilde{G}_{\phi z} & \tilde{G}_{\phi\phi} \end{bmatrix} = \begin{bmatrix} T_{11} & T_{12} \\ T_{21} & T_{22} \end{bmatrix} \begin{bmatrix} M_{11} & M_{12} \\ M_{21} & M_{22} \end{bmatrix}^{-1}$$

$$= \frac{1}{\Delta} \begin{bmatrix} T_{11}M_{22} - T_{12}M_{21} & -T_{11}M_{12} + T_{12}M_{11} \\ T_{21}M_{22} - T_{22}M_{21} & -T_{21}M_{12} + T_{22}M_{11} \end{bmatrix}$$

and Δ is the determinant of $\overline{\overline{M}}$.

Expanding the Green's functions, we have,

$$\tilde{G}_{zz} = \frac{1}{\Delta}\left\{-\left(\frac{k_{\rho 2}^3}{k_0^2}\right)\frac{J_n(k_{\rho 2}b)}{T_m(b)}\frac{T_m(\rho)}{T_e'(b)}V\right\}$$

where $V = \left[k_{\rho 1}^2 J_n'(k_{\rho 2}b)T_e(b) - k_{\rho 2}J_n(k_{\rho 2}b)T_e'(b)\right]$

$$\tilde{G}_{\rho z} = \frac{1}{\Delta}\left\{-\frac{k_z\beta_m}{j\varepsilon_r k_0^2}V1 + \frac{n\gamma_m k_{\rho 2}^2}{\omega\mu_0\rho}J_n(k_{\rho 2}b)T_e(\rho)\right\}$$

where $V1 = \left[k_{\rho 1}^2 T_e(b)\gamma_e - k_{\rho 2}^2 J_n(k_{\rho 2}b)\right]T_m'(\rho)$

$$\tilde{G}_{z\phi} = \frac{1}{\Delta}\left\{-n\left(\frac{k_{\rho 2}^2}{k_0^2}\right)\frac{k_z}{b}J_n(k_{\rho 2}b)\frac{T_m(\rho)}{T_m(b)}V2\right\}$$

where $V2 = \left[-J_n(k_{\rho 2}b) + J_n'(k_{\rho 2}b)\frac{T_e(b)}{T_e'(b)}\right]$

$$\tilde{G}_{\phi z} = \frac{1}{\Delta}\left\{\frac{nk_z(\varepsilon_r - 1)}{b}V3\right\} + \frac{nk_z}{\rho k_{\rho 1}^2}\tilde{G}_{zz}$$

where $V3 = \left(\frac{k_{\rho 2}^2}{k_{\rho 1}^2}\right)\left[J_n(k_{\rho 2}b)\right]^2\frac{T_e'(\rho)}{T_e'(b)}$

$$\tilde{G}_{\phi\phi} = \frac{1}{\Delta}\{\gamma_e T_e'(\rho)V4\} + \frac{nk_z}{\rho k_{\rho 1}^2}\tilde{G}_{z\phi}$$

where $V4 = \left[-k_{\rho 2}J_n'(k_{\rho 2}b) + \beta_m T_m'(b) - \frac{nk_z}{j\omega\mu_0 b}J_n(k_{\rho 2}b)\frac{\gamma_m}{\gamma_e}\right]$

$$\tilde{G}_{\rho\phi} = \frac{1}{\Delta}\left\{\frac{nk_z^2}{j\omega^2\varepsilon_r\varepsilon_0\mu_0 b} V5 + \frac{n^2 k_z}{\omega\mu_0 b\rho}\gamma_m J_n(k_{\rho 2}b)T_e(\rho)\right\}$$

$$+\frac{1}{\Delta}\left\{\frac{jn}{\rho}k_{\rho 2}\gamma_e J_n'(k_{\rho 2}b)T_e(\rho) - \frac{jn}{\rho}\beta_m\gamma_e T_m'(b)T_e(\rho)\right\}$$

where $V5 = \beta_m T_m'(\rho)\left[J_n(k_{\rho 2}b) - T_e(b)\gamma_e\right]$

And

$$\Delta = A - B$$

where

$$A = \left[\frac{1}{j\omega\mu_0}\left(k_{\rho 1}^2 T_e(b)\gamma_e - k_{\rho 2}^2 J_n\left(k_{\rho 2}b\right)\right)\right] V6$$

$$V6 = \left[-k_{\rho 2} J_n'\left(k_{\rho 2}b\right) + \beta_m T_m'(b) - \frac{nk_z}{j\omega\mu_0 b}\gamma_m T_e(b)\right]$$

$$B = \frac{nk_z k_{\rho 1}^2}{\omega^2\mu_0^2 b}\gamma_m T_e(b)\left[T_e(b)\gamma_e - J_n\left(k_{\rho 2}b\right)\right]$$

Over the surface $\rho = b$, we know that the tangential components of the electric field are zero over the patch and are non-zero elsewhere, while the surface current distribution is non-zero over the patch but zero otherwise. We can express the tangential electric field as :

$$\overline{E}_s(\rho=b)=\frac{1}{2\pi}\sum_{n=-\infty}^{\infty}\int_{-\infty}^{\infty}\left(\tilde{G}_{zz}\hat{z}+\tilde{G}_{\phi z}\hat{\phi}\right)\tilde{J}_{sz}e^{j(n\phi-k_z z)}dk_z$$

$$+\frac{1}{2\pi}\sum_{n=-\infty}^{\infty}\int_{-\infty}^{\infty}\left(\tilde{G}_{z\phi}\hat{z}+\tilde{G}_{\phi\phi}\hat{\phi}\right)\tilde{J}_{s\phi}e^{j(n\phi-k_z z)}dk_z \quad (5.11)$$

The surface current on the patch is expanded in terms of known basis functions, and after transforming it using (5.2), we have :

$$\tilde{J}_{sz}(n,k_z)=\sum_{p=1}^{N_z}I_{zp}\tilde{J}_{zp}(n,k_z)$$

$$\tilde{J}_{s\phi}(n,k_z)=\sum_{q=1}^{N_\phi}I_{\phi q}\tilde{J}_{\phi q}(n,k_z) \quad (5.12)$$

Substituting (5.12) into (5.11), we have the following expression :

$$\overline{E}_s(\rho=b)=\sum_{p=1}^{N_z}I_{zp}E_{zp}+\sum_{q=1}^{N_\phi}I_{\phi q}E_{\phi q} \quad (5.13)$$

where

$$E_{zp}=\frac{1}{2\pi}\sum_{n=-\infty}^{\infty}\int_{-\infty}^{\infty}\left(\tilde{G}_{zz}\hat{z}+\tilde{G}_{\phi z}\hat{\phi}\right)\tilde{J}_{zp}e^{j(n\phi-k_z z)}dk_z$$

$$E_{\phi p}=\frac{1}{2\pi}\sum_{n=-\infty}^{\infty}\int_{-\infty}^{\infty}\left(\tilde{G}_{z\phi}\hat{z}+\tilde{G}_{\phi\phi}\hat{\phi}\right)\tilde{J}_{\phi q}e^{j(n\phi-k_z z)}dk_z$$

By taking inner product with the same set of basis functions (i.e. $J_{zm}, J_{\phi m}$), and noting that the tangential electric field and the surface current are complementary that either one is zero anywhere on the surface at $\rho=b$, after using Parseval theorem, we arrive at a set of linear equations :

$$\sum_{p=1}^{N_z} I_{zp} Z_{mp}^{zz} + \sum_{q=1}^{N_\phi} I_{\phi q} Z_{mq}^{z\phi} = 0, \quad m = 1,2,\cdots,N_z$$

$$\sum_{p=1}^{N_z} I_{zp} Z_{mp}^{\phi z} + \sum_{q=1}^{N_\phi} I_{\phi q} Z_{mq}^{\phi\phi} = 0, \quad m = 1,2,\cdots,N_\phi \qquad (5.14)$$

where

$$Z_{mp}^{zz} = \sum_{n=-\infty}^{\infty} \int_{-\infty}^{\infty} \tilde{J}_{zm}(-n,-k_z)\tilde{G}_{zz}\tilde{J}_{zp}(n,k_z)dk_z$$

$$Z_{mq}^{z\phi} = \sum_{n=-\infty}^{\infty} \int_{-\infty}^{\infty} \tilde{J}_{zm}(-n,-k_z)\tilde{G}_{z\phi}\tilde{J}_{\phi q}(n,k_z)dk_z$$

$$Z_{mp}^{\phi z} = \sum_{n=-\infty}^{\infty} \int_{-\infty}^{\infty} \tilde{J}_{\phi m}(-n,-k_z)\tilde{G}_{\phi z}\tilde{J}_{zp}(n,k_z)dk_z$$

$$Z_{mq}^{\phi\phi} = \sum_{n=-\infty}^{\infty} \int_{-\infty}^{\infty} \tilde{J}_{\phi m}(-n,-k_z)\tilde{G}_{\phi\phi}\tilde{J}_{\phi q}(n,k_z)dk_z$$

We can rewrite (5.14) in matrix form for simplicity :

$$[Z][I]=0 \tag{5.15}$$

where

$$[Z]=\begin{bmatrix}[Z_{mp}^{zz}] & [Z_{mq}^{z\phi}]\\ [Z_{mp}^{\phi z}] & [Z_{mq}^{\phi\phi}]\end{bmatrix} \qquad [I]=\begin{bmatrix}[I_{zp}]\\ [I_{\phi q}]\end{bmatrix}$$

Nontrivial solutions can exist if the determinant of $[Z]$ is zero. The eigenvalue equation is :

$$\det(Z)=0 \tag{5.16}$$

The root of the eigenvalue equation is the complex resonant frequency we want.

We choose the sinusoidal function as basis functions.

$$\bar{J}_s=\hat{z}\sum_{p=1}^{N_z} I_{zp}J_{zp}+\hat{\phi}\sum_{q=1}^{N_\phi} I_{\phi q}J_{\phi q}$$

where

$$J_{zp}=\sin\left[\frac{2p-1}{L}\left(z-\frac{L}{2}\right)\pi\right]$$

$$J_{\phi q}=\sin\left[\frac{2q-1}{2\phi_0}(\phi-\phi_0)\pi\right]$$

3. NUMERICAL RESULTS

For the purpose of illustration, the resonance of TE_{01} (to z-direction) mode is studied. The dimensions of the patch are 3 cm by 4 cm, the inner radius of the cylinder is 5 cm, the substrate is of relative permittivity of 2.32. The current distribution is z-directed, it is found that only one mode of expansion function is sufficient, the resulting error of using 1 mode is 0.14 % compared with that of using 2 modes, and 0.24 % compared with that of using 3 modes.

	1 mode	2 modes	3 modes
Resonant Freq (GHz)	3.197591 + 6.2773456E-03*i	3.202172 + 6.2210825E-03*i	3.205115 + 6.2062214E-03*i

Figures 3 and 4 show the variations of of the complex resonant frequency with the thickness of the dielectric substrates with relative permittivity 2.32. It is observed that as the thickness increases, the real parts of the resonant frequencies drop monotonically, while the imaginary parts rise monotonically indicating that loss is larger for thicker substrates. As the thickness is approaching zero, the real parts of the resonant frequencies tend to 3.28 GHz, which is the same as the value predicted using a magnetic-wall cavity model similar to Krowne [7] :

$$f_{mn} = \frac{c}{2\sqrt{\varepsilon_r}}\sqrt{\left(\frac{m}{w}\right)^2 + \left(\frac{n}{L}\right)^2} \qquad (5.17)$$

where c is the speed of light in free space. The imaginary parts also tend to zero showing that there is no loss if the thickness of the cavity is vanishingly small.

Figure 5 shows the variation of Q-factor versus substrate thickness. The Q-factor is given as follows :

$$Q = \frac{Re(f)}{2\,Im(f)}$$

The Q-factor is found to increase with decreasing substrate thickness, especially as the thickness tends to zero, the Q-factor tends to a very large value as indicated by the above equation. Also the convergence behaviour of the solution is indicated in figure 5, the difference between the Q-factors calculated using only one or two modes of expansion functions is very small which further justifies the use of only one mode.

Muller's method is used to locate the complex zero of equation (5.16), the zero can usually be located within several iterations using the resonance frequency as calculated by equation (5.17) as the seed. An outline of algorithm using Muller's method is given in appendix B.

4. CONCLUSION

In this chapter, we have studied the resonance of a microstrip patch inside the inner surface of a hollow metallic cylinder rigorously using an spectral domain method. The resonance behaviour of TE_{01} mode is studied rigorously.

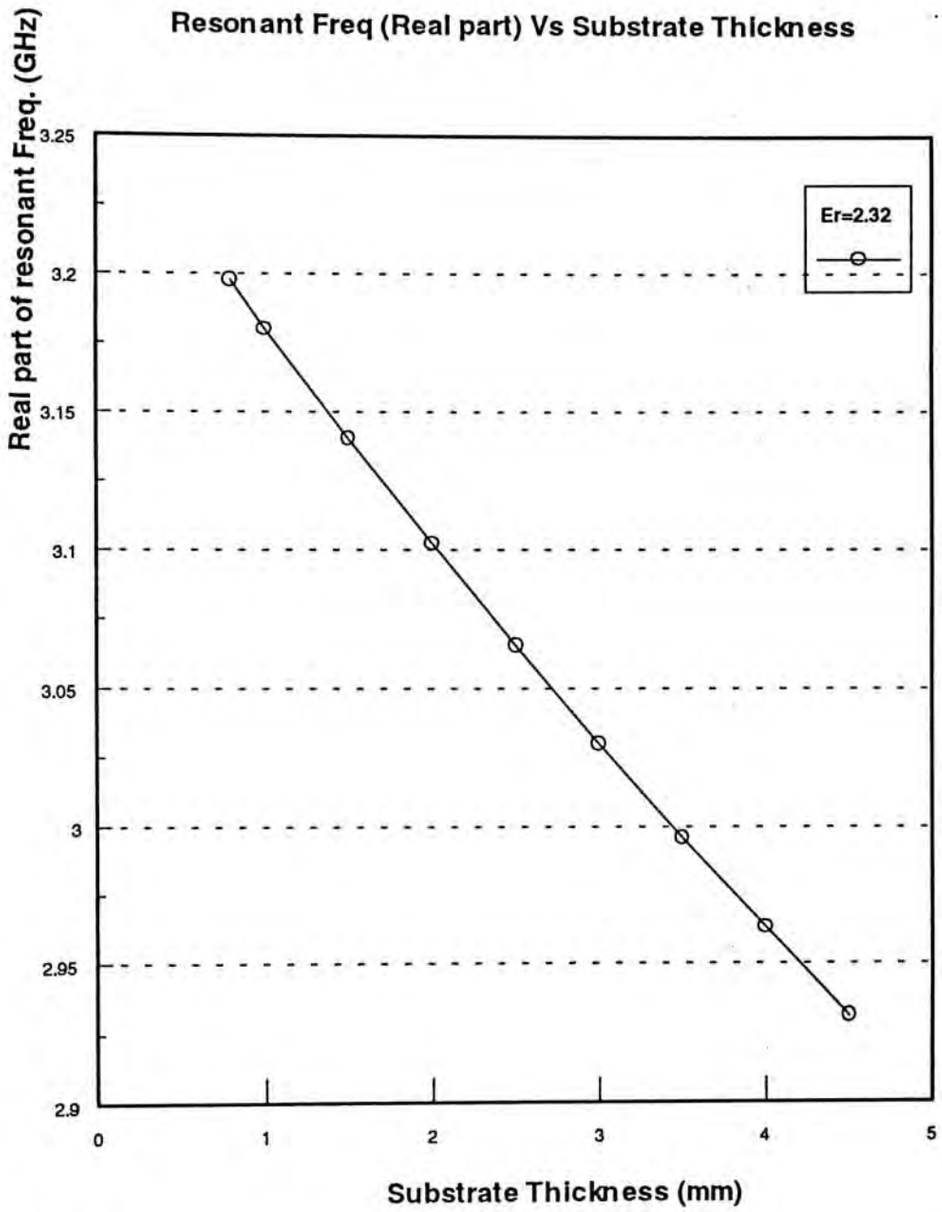

Figure 3 : The variations of real part of complex resonant frequency against substrate thickness : b = 5 cm, L=3cm, W=4cm, ε_r=2.32.

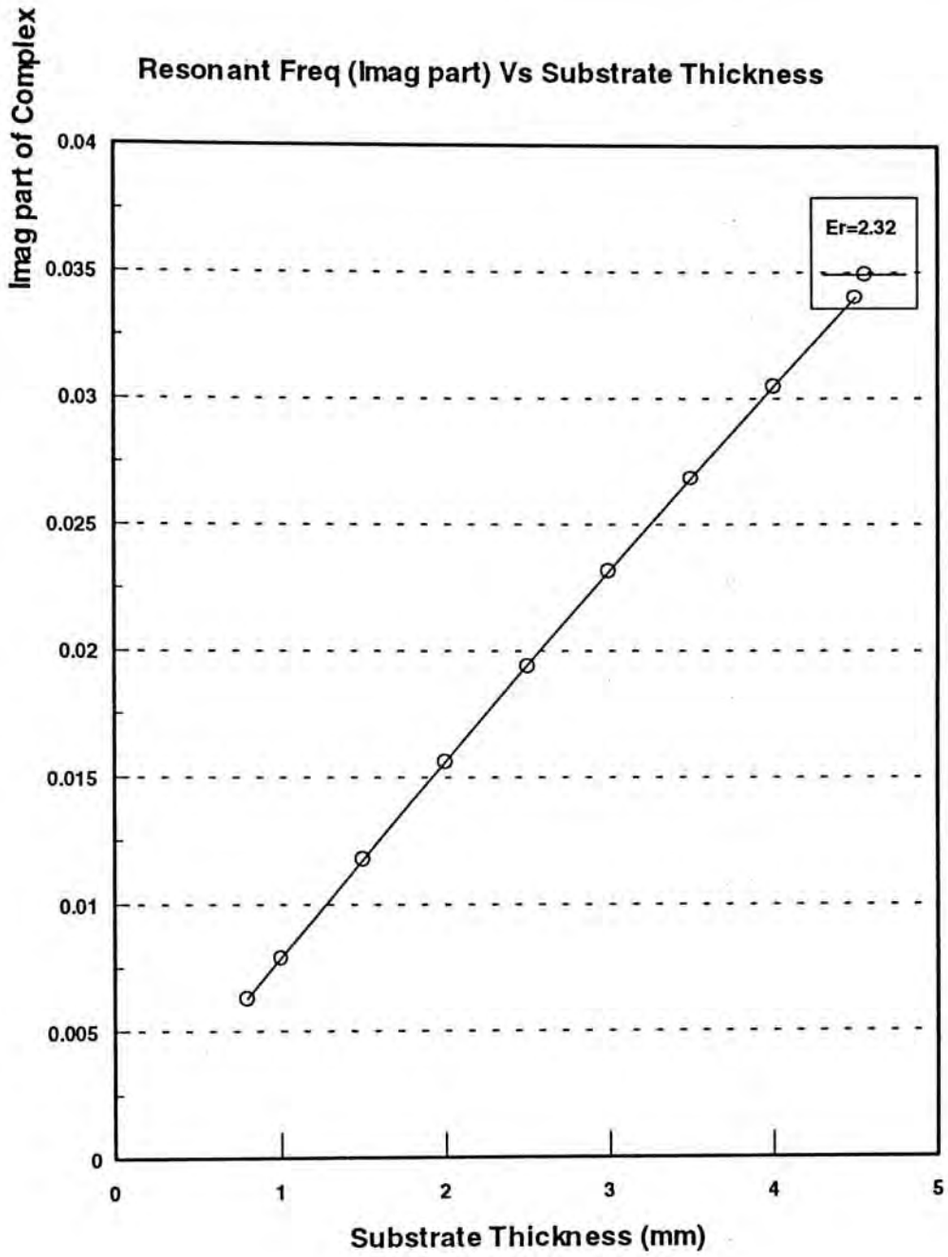

Figure 4 : The variations of imag part of complex resonant frequency against substrate thickness : b = 5 cm, L=3cm, W=4cm, ε_r=2.32.

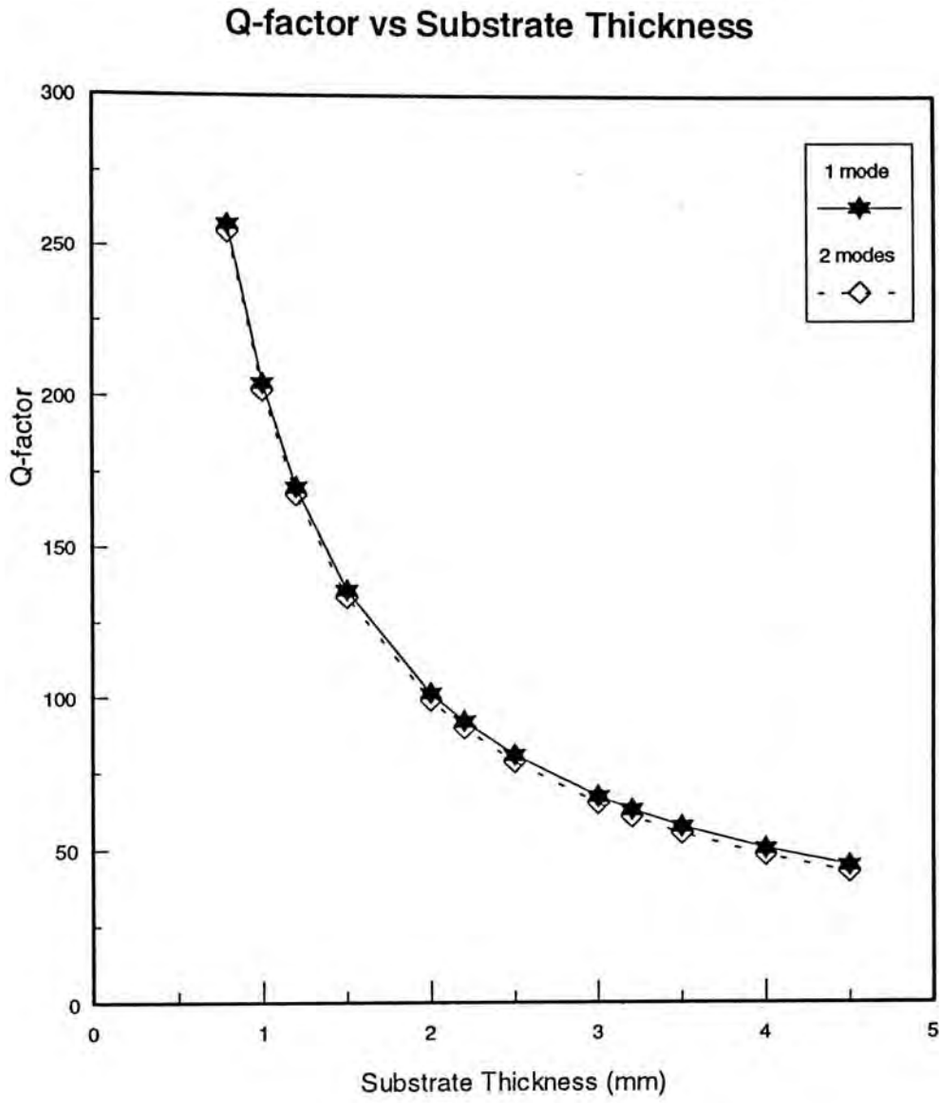

Figure 5 : The variations of Q-factor against substrate thickness : b = 5 cm, L=3cm, W=4cm, ε_r=2.32.

5. REFERENCES

1 R.E. Munson, "Conformal microstrip antennas and microstrip phased array," *IEEE Transactions on Antennas and Propagation*, vol. AP-22, pp.74-78, Jan. 1974.

2 I. Wolff and N. Knoppik, "Rectangular and circular microstrip disk capacitors and resonators," *IEEE Transactions on Microwave Theory and Techniques*, vol. MTT-22, pp. 857-864, 1974.

3 T. Itoh, "Analysis of microstrip resonators," *IEEE Transactions on Microwave Theory and Techniques*, vol. MTT-22, pp. 946-952, 1974.

4 W.C. Chew and J.A. Kong, "Resonance of the axial symmetric modes in microstrip disk resonators," *Journal of Mathematical Physics*, vol. 21, no. 3, pp. 582-591, 1980.

5 W.C. Chew and J.A. Kong, "Resonance of non-axial symmetric modes in circular microstrip disk resonators," *Journal of Mathematical Physics*, vol. 21, no. 10, pp. 2590-2598, 1980.

6 Y.T. Lo, D. Solomon, and W.F. Richards, " Theory and experiment on microstrip antennas," *IEEE Transactions on Antennas and Propagation*, vol. AP-27, pp. 137-145, 1979.

7 C.M. Krowne, "Cylindrical-rectangular microstrip antenna," *IEEE Transactions on Antennas and Propagation*, vol. AP-31, Jan. 1983.

8 S.M. Ali, T.M. Habashy, J.F. Kiang, and J.A. Kong, "Resonance in cylindrical-rectangular and wraparound microstrip structures," *IEEE Transactions on Antennas and Propagation*, vol. AP-37, no. 11, Nov. 1989.

9 J. Ashkenazy, S. Shtrikman, and D. Treves, "Electric surface current model for the analysis of microstrip antennas on cylindrical bodies," *IEEE Transactions on Antennas and Propagation*, vol. AP-33, no.3, Mar. 1985.

10 R.F. Harrington, *Time-Harmonic Electromagnetic Fields*, New York: McGraw-Hill, 1961. p. 202.

11 S.D. Conte, C. de Boor, *Elementary Numerical Analysis An Algorithmic Approach*, Third Edition, McGraw Hill, 1981. p.120-124

CHAPTER 6

INPUT IMPEDANCE OF RECTANGULAR MICROSTRIP ANTENNA INSIDE A METALLIC CYLINDER

1. INTRODUCTION

Input impedance of rectangular microstrip antenna mounted on cylindrical substrate has been studied by Luk et al. [1] using cavity model, and also by Habashy et al. [2] using moment method. However, the input impedance of a rectangular microstrip antenna mounted on the inner surface of a grounded metallic cylinder remains unreported. A method of calculating input impedance of a cylindrical-rectangular microstrip patch antennas will be covered in this chapter.

2. FORMULATION

A section of the antenna configuration is show in figure 1, the metallic cylinder is assumed to be infinitely long, and a layer of dielectric material is coated around the cylinder with a probe-fed patch radiator printed on its surface.

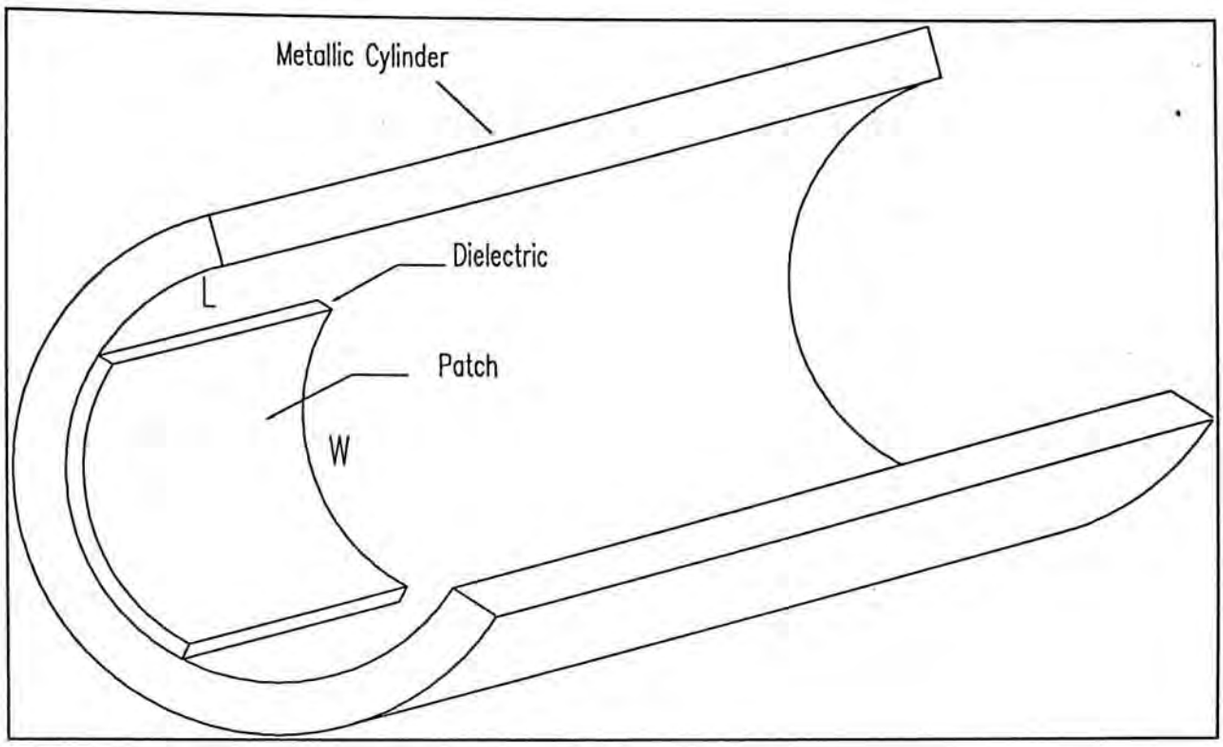

Figure 1 : The antenna configuration

Electric surface current model proposed by Ashkenazy et al. [3] is employed, an assumed surface current distribution is used to replace the printed radiator.

The method of analysis is similar to that in chapter 5. The spectral-domain Green's function of the configuration is derived by matching the boundary conditions. Note that the spectral-domain Green's function is the same as that derived in the previous chapter, so it is not repeated here.

The moment method solution employed here is a Galerkin's solution of the electric field integral equation. The unknown surface current density $\bar{J}_s(\phi, z)$ is expanded in a set of N basis functions.

$$\bar{J}_s(\phi, z) = \sum_{n=1}^{N} I_n \bar{J}_n(\phi, z)$$

Without loss of generality, the microstrip antenna is assumed to be probe-fed along the z-directed line of symmetry. The basis function is chosen as follows :

$$\bar{J}_n(\phi,z) = \hat{z}\cdot \sin\left[\frac{2m-1}{w}\left(z+\frac{w}{2}\right)\pi\right] \quad , m=1,2,3,\cdots$$

where w is the width of the patch.

Using the same set of test function as expansion function leads to a system of linear equation to be solved for the unknown current amplitudes I_n.

$$[Z][I]=[V]$$

where

$$Z_{mn} = -\int_{s_n} \bar{E}_m \cdot \bar{J}_n ds$$

$$V_m = -\int_{v_i} \bar{E}_m \cdot \bar{J}_i dv$$

$\bar{E}_m$ is the electric field due to the m-th test mode, $\bar{J}_i$ is the source current.

The input impedance is calculated using the following equation.

$$Z_{in} = \frac{-1}{I_i^2}\iiint_v \bar{E}\cdot\bar{J}_i dv$$

$$= -\sum_{n=1}^{N} I_n V_n$$

3. NUMERICAL RESULTS

Assuming that the coordinates of the feed-point is (ϕ_f, z_f), where the point (0,0) is the center of the patch. For the purpose of illustration, the feed-point is located at $\phi_f = 0, z_f = -1\text{cm}$.

Figure 2 shows the convergence check for the moment method solution, it is found that the variation in resonant frequency between four and one expansion mode is only 0.3%, the convergence is so good that only one-term approximation is quite good already for the above configuration.

Figures 3 and 4 show the variations of impedance level with the feed point, three sets of data are plotted, with z_f =-0.2, -0.5 and -1.0 cm respectively. It is found that by varying the feed-point from the center of patch approaching to the edge, the impedance level rises, hence impedance matching is possible.

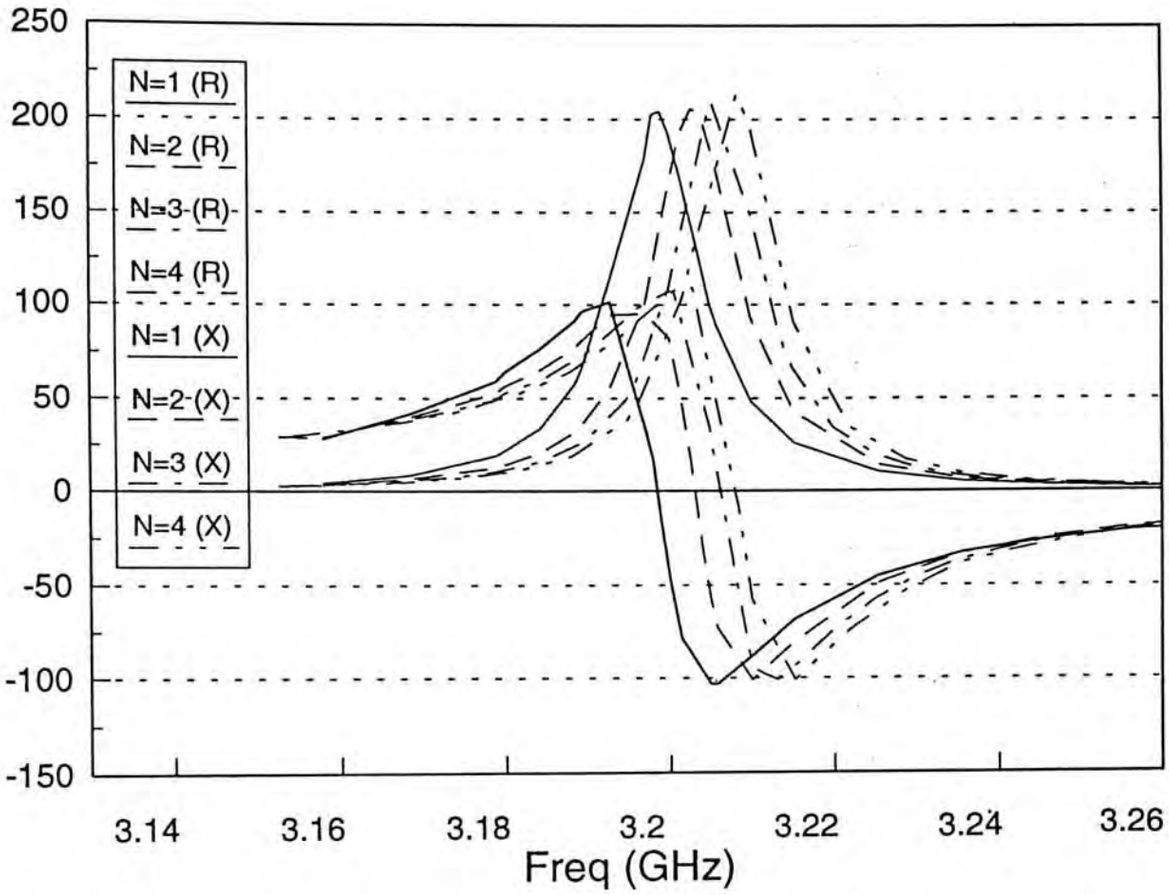

Figure 2 : Convergence check

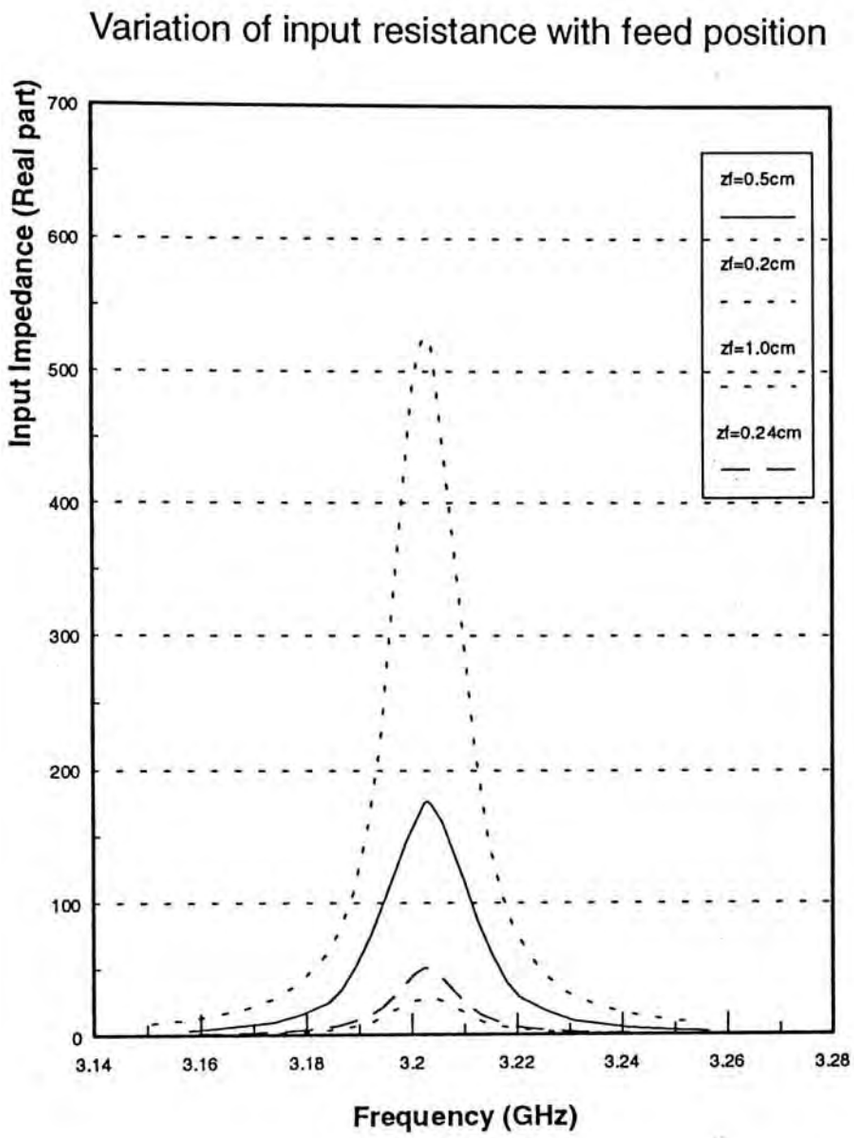

Figure 3 : Variations of Input resistance against the probe feed-position.

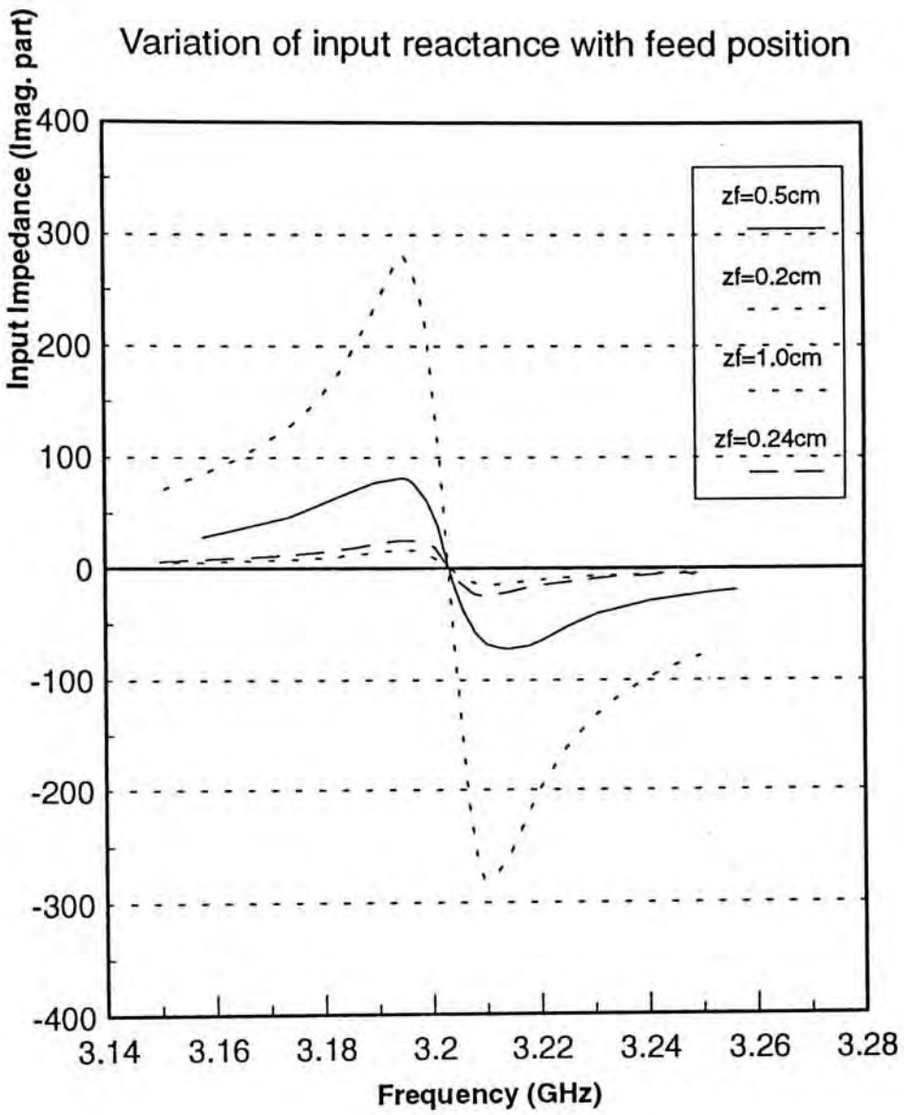

Figure 4 : Variations of Input reactance against the probe feed-position.

4. CONCLUSION

A method of computing input impedance of a rectangular microstrip antenna inside a metallic cylinder has been covered in this chapter. The method makes use of electric surface current model and moment method. It is shown that impedance matching is possible by choosing suitable feed-point of the probe.

5. REFERENCES

1. K.M. Luk, K.F. Lee, J.S. Dahele, 'Analysis of the Cylindrical-Rectangular Patch Antenna', *IEEE Trans Antennas Propagat.*, vol. 37, No. 2, Feb 1989.

2. T.M. Habashy, S.M. Ali, J.A. Kong, 'Input Impedance and Radiation Pattern of Cylindrical-Rectangular and Wraparound Microstrip Antennas', *IEEE Trans Antennas Propagat.*, vol.,38, No.5, May 1990.

3. J. Ashkenazy, S. Shtrikman, D. Treves, 'Electric Surface Current Model for the Analysis of Microstrip Antennas on Cylindrical Bodies', *IEEE Trans Antennas Propagat.*, vol.33, No.3, Mar 1985.

CHAPTER 7

SUMMARY

Summary of Works

An algorithm of computing integer order Bessel function, Neumann function, and Hankel functions over wide range of complex arguments. The program developed was tested using Mathematica 1.2. It has been that the algorithms described give good results, even for extremely large argument.

An alternative method of computing input impedance of cylindrical-rectangular microstrip antenna has been proposed, and results have been checked with experimental data from Dahele et. al. Excellent agreement between theory and experiment is achieved.

An analysis of mutual impedance between cylindrical-rectangular microstrip antennas has been made. The effects of variation of patch separations, relative permittivity, dielectric thickness have been studied.

The resonance of a microstrip patch inside the inner surface of a hollow metallic cylinder has been rigorously studied using an spectral domain method.

A method of computing input impedance of a rectangular microstrip antenna inside a metallic cylinder has been studied. It is shown that impedance matching is possible by choosing suitable feed-point of the probe.

Further Works

Although excellent agreements between theory and experiments in literature have been obtained, the author noticed a significant deviations of impedance level in input impedance measurements, but the agreement in resonant frequency has been excellent. This can be a possible topic of research.

Besides, the analysis has been limited to small cylinder, there are still much room for research concerning large cylinders. Alternative methods can be used for the analysis, for example, finite difference.

APPENDIX A

Galerkin's method

In the previous chapters, we can derive the green's functions in spectral domain, and so we can relate the electric field components in spectral domain to the spectral domain surface current distribution. However, both the surface current and the electric field are unknown entities. Galerkin's method has been used to convert the equations into a matrix equation to solve for the unknowns. A brief summary of Galerkin's function will be covered in this appendix.

Given an operator equation of the following form :

$$LX=Y \qquad (1)$$

where A is a linear operator and X is an unknown to be determined for a particular excitation or forcing function Y.

Galerkin's method starts by expanding X using a set of *known* basis function or expansion functions x_i with *unknown* coefficients a_i . Or mathematically,

$$X = \sum_{i=1}^{\infty} a_i x_i \qquad (2)$$

Since it is impossible to implement infinite summation numerically, we have to truncate the infinite summation after a finite number of term N.

$$X \approx X_N = \sum_{i=1}^{N} a_i x_i \tag{3}$$

Substituting equation (3) into equation (1) yields

$$\begin{aligned} LX_N &= \sum_{i=1}^{N} a_i L x_i \\ &= Y_N \approx Y \end{aligned} \tag{4}$$

The residue R_N is defined as

$$\begin{aligned} R_N &= LX_N - Y \\ &= Y_N - Y \end{aligned} \tag{5}$$

and the residue is weighted (by taking inner product) to zero with respect to a weighting function or testing function w_i. In Galerkin's method, the weighting function w_i is chosen to be identical to the basis function x_i.

$$\langle R_N, x_j \rangle = 0 \qquad j = 1,2,...,N \tag{6}$$

The inner product can be defined as

$$\langle X_1, X_2 \rangle = \int_l X_1 \cdot X_2 dz \tag{7}$$

where l is the domain of the operator L.

Equation (6) can be rewritten as follows :

$$\left\langle \sum_{i=1}^{N} a_i L x_i, x_j \right\rangle = \langle Y, x_j \rangle \qquad j = 1,2,\ldots,N$$

$$\sum_{i=1}^{N} a_i \langle L x_i, x_j \rangle = \langle Y, x_j \rangle \qquad (7)$$

Equation (7) can be written in matrix form :

$$[l_{ji}][a_i] = [y_j]$$

where

$$[l_{ji}] = \begin{bmatrix} \langle x_1, Lx_1 \rangle & \langle x_1, Lx_2 \rangle & \cdots & \langle x_1, Lx_N \rangle \\ \langle x_2, Lx_1 \rangle & \ddots & & \vdots \\ \vdots & & \ddots & \vdots \\ \langle x_N, Lx_1 \rangle & \cdots & \cdots & \langle x_N, Lx_N \rangle \end{bmatrix}$$

$$[a_i] = \begin{bmatrix} a_1 \\ a_2 \\ \vdots \\ a_N \end{bmatrix}, \qquad [y_j] = \begin{bmatrix} \langle x_1, Y \rangle \\ \langle x_2, Y \rangle \\ \vdots \\ \langle x_N, Y \rangle \end{bmatrix}$$

If $[l_{ji}]$ is non-singular, then

$$[a_i] = [l_{ji}^{-1}][y_j]$$

And define $[\tilde{X}_n] = [x_1 \quad x_2 \quad \cdots \quad x_N]$

The solution for the unknown X is

$$X = [\tilde{X}_i][l_{ji}^{-1}][y_j]$$

APPENDIX B

MULLER'S METHOD

Muller's method can be used to find any prescribed numbers of zeros, real or complex, of an arbitrary function. It is an iterative approach that converges almost quadratically in the vicinity of a zero, and it does not require the evaluation of the derivatives of the function. The method is global in the sense that the user does not have to provide an initial guess for the algorithm to start.

An algorithm for Muller's method is shown below :

1. Let x_0, x_1, x_2 be three approximations to a zero ξ of f(x). Compute $f(x_0)$, $f(x_1)$ and $f(x_2)$.

2. Compute

   $h_2 = x_2 - x_1$, $h_1 = x_1 - x_0$

   $f(x_2, x_1) = (f(x_2) - f(x_1)) / h_2$

   $f(x_1, x_0) = (f(x_1) - f(x_0)) / h_1$

3. Set i = 2

4. Compute

   $f[x_i, x_{i-1}, x_{i-2}] = (f[x_i, x_{i-1}] - f[x_{i-1}, x_{i-2}]) / (h_i + h_{i-1})$

$c_i = f[x_i, x_{i-1}] + h_i f[x_i, x_{i-1}, x_{i-2}]$

5. Compute

$$h_{i+1} = -2f(x_i) / \left(c_i \pm \sqrt{c_i^2 - 4f(x_i)f[x_i, x_{i-1}, x_{i-2}]}\right)$$

Choose the sign so that the denominator is largest in magnitude.

6. Set $x_{i+1} = x_i + h_{i+1}$

7. compute

$f(x_{i+1})$ and $f(x_{i+1}, x_i) = (f(x_{i+1}) - f(x_i)) / h_{i+1}$

8. Set $i = i + 1$ and repeat steps 4-7 until either of the following criteria is satisfied for the tolerance ε_1, ε_2 :

- $|x_i - x_{i-1}| < \varepsilon_1 |x_i|$
- $|f(x_i)| < \varepsilon_2$

or until the maximum number of iterations is exceeded.

PUBLICATION LIST :

1 W.P. Tan, K.Y.A. Lai, "The computation of Bessel functions and Hankel functions for integer orders and complex arguments", accepted for publication in *International Journal of Electronics*.

2 W.P. Tan, K.Y.A. Lai, "Input impedance of rectangular microstrip antenna Mounted inside a metallic cylindrical ground plane", presented in Asia Pacific Microwave Conference 1993.

3 W.P. Tan, K.Y.A. Lai, "Resonance of microstrip patch inside a hollow metallic cylinder", submitted to *IEE Proceedings-H*.